Progress in Neurobiology 208 (2022) 102173

Contents lists available at ScienceDirect

Progress in Neurobiology

journal homepage: www.elsevier.com/locate/pneurobio

P2X7 receptor blockade reduces tau induced toxicity, therapeutic implications in tauopathies

Caterina Di Lauro [a,b], Carolina Bianchi [a,b], Álvaro Sebastián-Serrano [a,b], Lucia Soria-Tobar [a], Beatriz Alvarez-Castelao [a], Annette Nicke [c], Miguel Díaz-Hernández [a,b,*]

[a] Department of Biochemistry and Molecular Biology, Veterinary School, Complutense University of Madrid, Avda. Puerta De Hierro S/N, 28040, Madrid, Spain
[b] Instituto de Investigación Sanitaria del Hospital Clínico San Carlos, IdISSC, Madrid, Spain
[c] Walther Straub Institute of Pharmacology and Toxicology, Faculty of Medicine, Ludwig-Maximilians-Universität München, Munich, Germany

ARTICLE INFO

Keywords:
Alzheimer disease
Pick disease
Neuroinflammation
ATP
P2X7

ABSTRACT

Tauopathies are neurodegenerative diseases characterized by the presence of aberrant intraneuronal aggregates of hyperphosphorylated Tau protein. Recent studies suggest that associated chronic neuroinflammation may contribute to the pathological Tau dissemination. However, the underlying molecular mechanisms remain unknown. Since purinergic P2X7 receptors (P2X7) can sense the rise of extracellular ATP levels associated with neuroinflammation, its involvement in neurodegeneration-associated inflammation was suggested. We found a P2X7 upregulation in patients diagnosed with different tauopathies and in a tauopathy mouse model, P301S mice. *In vivo* pharmacological or genetic blockade of P2X7 reverted microglial activation in P301S mice leading to a reduction in microglial migratory, secretory, and proliferative capacities, and promoting phagocytic function. Furthermore, it reduced the intraneuronal phosphorylated Tau levels in a GSK3-dependent way and increased extracellular phosphorylated Tau levels by reducing the expression of ectoenzyme TNAP. Accordingly, pharmacological or genetic blockade of P2X7 improved the cellular survival, motor and memory deficits and anxiolytic profile in P301S mice. Contrary, P2X7 overexpression caused a significant worsening of Tau-induced toxicity and aggravated the deteriorated motor and memory deficits in P301S mice. Our results indicate that P2X7 plays a deleterious role in tauopathies and suggest that its blockade may be a promising approach to treat Tauopathies.

1. Introduction

Tauopathies are a family of neurodegenerative disorders characterized by the presence of aberrant intraneuronal aggregates of hyperphosphorylated microtubule-associated protein Tau. Tauopathies include, among others, Alzheimer's disease (AD) and Pick's disease (PiD) (Lee et al., 2001). In both diseases, Tau-associated pathology progression correlates with neuronal loss, neuroinflammation and cognitive decline (Bondareff et al., 1989; Lee et al., 2001). Emerging pieces of evidence suggest that abnormal Tau accumulation is mediated through the spreading of Tau protein from cell to cell. In agreement with this hypothesis, it was reported that Tau protein can be released into the extracellular space through physiological and pathological mechanisms. In the brain parenchyma, Tau protein can be toxic for neighbouring cells and, in this way, promotes the spread of Tau-induced toxicity (Gomez-Ramos et al., 2006; Sebastian-Serrano

Abbreviations: AD, Alzheimer's Disease; APP, Amyloid Precursor Protein; ATP, Adenosine-5′-triphosphate; Aβ, amyloid-β peptide; CSF, Cerebrospinal fluid; DAMPs, Damage-associated molecular patterns; EGFP, Enhanced green fluorescent protein; GSK3, Glycogen synthase kinase 3; Iba-1, Ionized calcium binding adaptor molecule 1; IL-1, Interleukin-1; IL-1R, Interleukin-1 receptor; IL-1β, Interleukin-1β; IL-6, Interleukin-6; LPS, Lipopolysaccharide; MAPT, Microtubule-associated protein tau; mRNA, Messenger ribonucleic acid; NLRP3, NLR Family Pyrin Domain Containing; P2X7, Purinergic receptor P2X7; PBS, Phosphate-buffered saline solution; PiD, Pick's Disease; Prnp, Prion protein promoter; SEM, Standard error of the mean; TNAP, Tissue-Nonspecific Alkaline Phosphatase; TNFα, Tumor necrosis factor; WT, Wild-Type; eTau, extracellular Tau protein.

* Corresponding author at: Dpto. Bioquímica y Biología Molecular, Facultad de Veterinaria, Universidad Complutense de Madrid, Avenida Puerta de Hierro s/n, 28040, Madrid, Spain.
E-mail address: migueldiaz@ucm.es (M. Díaz-Hernández).

https://doi.org/10.1016/j.pneurobio.2021.102173
Received 23 March 2021; Received in revised form 2 September 2021; Accepted 7 September 2021
Available online 10 September 2021

et al., 2018a). Further studies proposed that neuroinflammation associated with neurodegeneration also contributes to pathological Tau dissemination (Asai et al., 2015; Maphis et al., 2015; Yoshiyama et al., 2007).

Neuroinflammation is an active inflammatory response characterized by the production of inflammatory mediators and mainly mediated by microglia cells. Under non-pathological conditions, microglia cells show a highly ramified shape that allows them to screen the brain parenchyma for invading pathogens or damage-associated molecular patterns (DAMPs) (Colonna and Butovsky, 2017). In neurodegenerative diseases, damaged or dying cells release DAMPs that cause microglial activation, which is characterized by an amoeboid shape with fewer and shorter ramifications (Skaper et al., 2018). When microglia remain activated over time, the continued release of pro-inflammatory cytokines negatively affects neural cells which release more DAMPs, thereby accelerating the inflammatory process and leading to a chronic neuroinflammation state (Heneka et al., 2018). However, neither the molecular mechanisms nor the effectors causing the chronic microglial activation are well known at this time.

In Tauopathies, microglial activation correlates with the spread of Tau pathology in the anatomically connected regions of the hippocampus (Maphis et al., 2015). Administration of immunosuppressors attenuated the Tau associated pathology in the well-characterized P301S tauopathy mouse model. These mice express 5-fold more Tau protein and show an onset of phospho-tau pathology at around 6 months of age in the absence of amyloid-β (Aβ) plaques (Yoshiyama et al., 2007). Similarly, another work reported that microglial depletion halted Tau spreading (Asai et al., 2015). All these findings suggest that alterations in neuron-microglia interaction play a critical role in the spread of Tau pathology. Supporting this hypothesis, the blockage of inflammatory cytokine interleukin-1 (IL-1) by the administration of IL-1R1 antagonist (interleukin 1 receptor, type 1) reduced microglia-induced Tau pathology (Maphis et al., 2015), whereas the conditional overexpression of IL-1β raised the pathological Tau phosphorylation (Ghosh et al., 2013). Based on these findings, the reversion of chronic neuroinflammation associated with Tauopathies may be considered a potential therapeutic strategy to reduce Tau-induced toxicity.

Several reports suggest that elevated extracellular ATP behaves as a DAMPs and is sensed by the purinergic P2X7 receptor (Burnstock, 2007; Roh and Sohn, 2018). P2X7 was described in almost all brain cellular lineages including microglia and neurons (Miras-Portugal et al., 2017). In neurons, P2X7 has been reported to show a critical role in relevant physiological events including axonal growth and branching, neurotransmitter release, and neuronal differentiation (Miras-Portugal et al., 2017). Moreover, its activation was shown to promotes intraneuronal Tau phosphorylation *via* GSK3 kinase (Diaz-Hernandez et al., 2008). In microglia cells, P2X7 was found to regulate migration, proliferation (Martinez-Frailes et al., 2019; Rigato et al., 2012; Sanz et al., 2009), and phagocytosis (Gu and Wiley, 2018; Martinez-Frailes et al., 2019; Ni et al., 2013). Besides, microglial P2X7 activation promotes NLPR3 inflammasome assembly, resulting in IL-1β maturation and release (Facci et al., 2018; Monif et al., 2010). Sustained inflammasome activation is postulated to contribute to chronic neuroinflammation associated with neurodegenerative diseases (Heneka et al., 2018). In accordance, increased P2X7 expression was found in microglial cells in AD patients (Martin et al., 2019; Martinez-Frailes et al., 2019; McLarnon et al., 2006; Parvathenani et al., 2003). Furthermore, a higher binding of a selective P2X7 radiotracer was observed in hippocampal glial cells of P301S mice (Jin et al., 2018). Although all these studies suggest a contribution of P2X7 to Tau-induced neuroinflammation, no substantial evidence has been provided yet.

In this study, we therefore examined whether P2X7 contributes to Tau-induced pathology. We detected increased levels of both protein and mRNA levels of P2X7 in post-mortem brain from patients with distinct Tauopathies. Brain samples from P301S mice showed a similar rise of microglial P2X7 levels that impacted on the microglial functionality. Most importantly, genetic or pharmacological inactivation of P2X7 in P301S mice as well as its overexpression support our hypothesis that selective P2X7 antagonists that are permeable to the blood-brain barrier represent a novel and promising therapeutic strategy to treat these diseases.

2. Materials and methods

2.1. Human brain tissues

Human samples were provided by the Banco de Tejidos Fundación CIEN (BT-CIEN, Madrid, Spain). A written informed consent for brain removal after death for diagnostic and research purposes was obtained from the brain donors and/or next of kin. Procedures, information and consent forms were approved by the Bioethics Subcommittee of Fundación Cien Madrid, Spain (S19001). Supplementary Table 1 summarizes the gender and age of the patients with AD or PiD from whom the hippocampal post-mortem samples were collected.

2.2. Animals

All animal procedures were carried out at the Universidad Complutense de Madrid (UCM), in compliance with National and European regulations (RD1201/2005; 86/609/CEE) and following the guidelines of the International Council for the Laboratory Animal Science. The protocol for animal experiments was approved by the Committee of Animal Experiments at the UCM and the Environmental Counselling of the Comunidad de Madrid, Spain (PROEX 374/15 and PROEX 185/17).

The P301S mice were obtained from Jackson laboratory [line B6; C3-Tg (Prnp-MAPT*P301S)PS19Vle/J; stock number 008169]. The original B6C3H/F1 genetic background was changed to C57BL/6 J by backcrossing them with C57 animals in our laboratory. The P301S model is a transgenic line carrying the human 1N4R MAPT gene with the P301S mutation under the control of the mouse prion protein promoter (Prnp).

P2X7 null mice ($P2X7^{-/-}$, B6N-P2rx7tm1d(EUCOMM)Wtsi/Ieg) and overexpressing EGFP-tagged P2X7 ($P2X7^{451P}$-EGFP, B6N-Tg (RP24-114E20-P2X7451 P/StrepHisEGFP)17Ani) mice were generated by Prof. Annette Nicke as previously described (Kaczmarek-Hajek et al., 2018). Heterozygous P301S mice (P301S) were crossed with $P2X7^{-/-}$ and $P2X7^{451P}$-EGFP mice, and subsequently back-crossed to finally obtain double P301S; $P2X7^{-/-}$ and P301S;$P2X7^{451P}$-EGFP.

Heterozygous P301S mice were also crossed with a transgenic mouse line expressing EGFP protein immediately downstream of P2X7 promoter, ^{P2X7}EGFP Tg(P2rx7-EGFP)FY174Gsat/Mmcd, stock 011959-UCD (Sebastian-Serrano et al., 2016).

Animals were housed in a light and temperature-controlled humid environment, with a 12 h light-dark cycle and a light onset at 08:00 am. The mice were grouped 4–6 per cage and allowed free access to water and food (*ad libitum*). All surgeries were performed under isoflurane anesthesia, and all efforts were made to minimize suffering. Investigators were blinded to the group allocation during the animal experiments.

We used 21 wild-type mice (WT), 10 females and 11 males; 26 P301S mice, 14 females, and 12 males; 6 P301S; $P2X7^{-/-}$ 3 females, and 3 males; 5 P301S;P2X 7^{451P}-EGFP, 3 females, and 2 males; 6 $P2X7^{451P}$-EGFP, 3 male and 3 female. When the animals were divided into the different groups for whatever procedure, we kept the gender variable balanced among all groups.

2.3. PCR genotyping

Genomic DNA was obtained from tail biopsies using Wizard® SV Genomic DNA Purification System (Promega, Madison, WI, United States) according to the manufacturer's protocol.

Simple PCR reactions were carried out using: for P301S mice DNA Kapa2G Fast HS Master Mix from Sigma-Aldrich (Madrid-Spain), specific primers (0.5 μM each) and 2 μL of genomic DNA in a final volume

of 12 μL; for P301S;P2X7$^{-/-}$ and P301S;P2X7^{451P}-EGFP mice Econo PLUS Green 2x Master Mix, specific primers (10 μM each) and 1 μL of genomic DNA in a final volume of 25 μL; for ^{P2X7}EGFP mice DNA Amplitools Master Mix (Biotools, Madrid, Spain), specific primers (0.4 μM each) and 5 mL of genomic DNA in a final volume of 25 μL. Animals were genotyped using specific primers for P301S Fw 5′-GGC ATC TCA GCA ATG TCT CC-3′ and Rv 5′-GGT ATT AGC CTA TGG GGG ACAC-3′; for *P2rx7*$^{-/-}$ Fw 5′-CTGGCAACTATCCATTTTCC-3′ and Rv 5′-GTGTGAGTGAATGAGATCGTG-3′; for *PX7*^{451P}*-EGFP* Fw 5′-GGT TCT TAG CAG GCT TAA CAG CA-3′ and Rv 5′-ATG GGG GTG TTC TGC TGG TAG T-3′; for ^{P2X7}EGFP Fw 5′−CCTACGGCGTGCAGTGCTTCAGC-3′ and Rv 5′-CGGCGAGCTGCACGCTGCGTCCTC-3′. PCR was carried out over 28 cycles 94 °C for 15 s, 65 °C for 15 s, 72 °C for 10 s for P301S primers; over 35 cycles 94 °C for 30 s, 60 °C for 1 min, 72 °C for 1 min for P2X7^{451P}-EGFP primers; over 35 cycles 94 °C for 30 s, 60 °C for 1 min, 72 °C for 1 min and 45 s for P2X7$^{-/-}$ primers; over 40 cycles of 94 °C for 30 s, 60 °C for 45 s, and 72 °C for 45 s for EGFP primers.

PCR amplification products were electrophoresed on a 1.5 % (w/v) agarose gel and stained with SYBR® Safe DNA Gel Stain (Life Technologies CA, USA). PCR bands were visualized by gel imaging system Gel Logic 200 Imaging System (Kodak, Rochester, NY, USA).

2.4. RNA extraction and quantitative real-time PCR (qRT-PCR)

Total RNA was extracted from hippocampi from human or adult mouse brains using a Speedtools total RNA Extraction Kit (Biotools) and following the manufacturer's instructions. The animals were quickly sacrificed, and the hippocampi were immediately dissected and frozen using dry ice to proceed with total RNA isolation. After digestion with TURBO DNase (Ambion), 1 μg of total RNA was reverse transcribed with 6 μg of random primers, 350 μM dNTPs and M-MLV reverse transcriptase (all from Invitrogen).

qRT-PCR reaction mixtures containing DNA Master SYBR Green I mix (Applied Biosystems) were incubated at 95 °C for 20 s followed by 40 PCR cycles (95 °C for 1 s and 60 °C for 20 s) in a StepOnePlus Real-Time PCR System (Applied Biosystems). The specific primers for human *P2RX7* were Fw 5′- AAAACAGAAGGCCAAGAGCA-3′ and Rv 5′- CACCAGGCAGA-GACTTCACA-3′, for mouse *P2rx7* Fw 5′- GGTGCCAGTGTGGAAATTG-3′ and Rv 5′- TAGGGATACTTGAAGCCACT-3′; and for *GAPDH* or *Gapdh* Fw 5′-CACCACCAACTGCTTAGCCC-3′ and Rv 5′-TGTGGTCATGAGCCCTTCC -3′. Expression levels of mRNA were represented as $2^{-\Delta\Delta Ct}$, where average cycle threshold (Ct) was obtained from triplicates of each sample. First, ΔCt means were normalized to parallel amplification of GAPDH as endogenous control. Next, ΔΔCt means were normalized to the average of corresponding controls.

2.5. Drug preparation and administration

P2X7 specific negative allosteric antagonist GSK 1482160A was diluted at 10 mg/mL in vehicle solution. Vehicle solution was calcium- and magnesium-free sterile phosphate buffered saline (PBS) plus 20 % hydroxypropyl-β-cyclodextrin and 0.2 % DMSO. 10 μL of GSK solution corresponding to a dosage of 100 mg per Kg of body weight or the same volume of vehicle solution were daily intraperitoneally injected to 9-months-old P301S and WT mice per three weeks. The treatment protocol followed a single-blind design, by which the experimenter was unaware of the genotype and treatment applied to each mouse (n = 6–7 mice per group and condition). After treatment, mice were sacrificed, and brain tissue was processed to perform immunoblot and immunohistochemical analyses.

In vivo LPS-treatment was done as previously described (Martinez--Frailes et al., 2019).

2.6. Behavioral assay

All mice were handled for at least 3–4 consecutive days before testing. They were tested in random order and the experimenter conducting the tests was unaware of the genotype/group. All behavioural devices were located in a sound-proof room and the experimental area was homogeneously illuminated around 70 lx. All apparatus was carefully cleaned with alcohol (70 ° proof) after each session.

Open field test: is an experimental test used to assay general locomotor activity levels, anxiety, and willingness to explore a novel environment. The apparatus consists of a standard clear plastic tank (42cm × 42cm). There is no need to habituate the mouse before the test. A single adult mouse was gently placed into the setup and its position was video tracked for 10 min. The analysis consisted of measuring the amount of time spent by the mouse in the centre (17 × 17 cm) of the tank and in the periphery (the surrounding area of the arena). The tendency to avoid the centre of a novel environment and remain close to the wall of the tank is an index of anxiety. Data acquisition and analysis were performed automatically using Any-Maze software (Stoelting Co, Wood Dale, IL, USA).

Elevated plus maze test: is a test measuring the anxiety and is based on the animal's aversion to open spaces. The test uses an elevated, plus-shaped (+) apparatus with two open and two enclosed arms. There is no need to habituate the mouse before the test. A single adult mouse was gently placed into the centre of setup (at the intersection of the open and enclosed arms) and its position was video tracked for 5 min. The analysis consisted of measuring the amount of time spent by the mouse in the different arms using Any-Maze software.

Rotarod: this test is used to measure coordination and balance. The test requires a special apparatus capable of rotating at speeds between 4 and 40 rpm. Mice needed to be trained during two days before the test (first day: 4 rpm for 1 min, 4 repetitions; second day: 4–8 rpm for 2 min, 4 repetitions). After this trial the rod was set to accelerate from 4 to 40 rpm over 5 min for 4 repetitions. The amount of time which elapsed from when the mice fell off was recorded and the average of the 4 rounds was calculated.

Novel object recognition test: this test is commonly used to test the ability of learning and memory in animals. The test consisted of a training phase, during which the mice were trained to explore two identical objects for ten minutes, and a testing phase (10 min) during which one of the familiar objects was replaced with a new one. A normal animal should spend more time investigating the new object instead of the familiar one. Time spent exploring the different objects was recorded and analyzed using Any-Maze software.

2.7. Collection of cerebrospinal fluid (CSF) samples

CSF samples from all genotypes and condition were randomly collected in a blinded way as previously described (Sebastian-Serrano et al., 2018b). Briefly, mice were anesthetized with isoflurane diluted in 50 % O_2 and placed in a stereotaxic frame with the head forming a near 135° angle with the body. Mice were kept under anaesthesia during the surgery. The CSF was collected from the cisterna magna with a pulled capillary. Blood vessels were carefully avoided when penetrating the dura mater with the capillary tube in order to prevent contamination by plasma proteins. CSF was immediately frozen on dry ice.

2.8. Phagocytosis assay

In vivo phagocytosis assays were done as previously described (Martinez-Frailes et al., 2019). 9-month-old WT and P301S mice treated either with vehicle and GSK solution were randomly anesthetized with isoflurane (1-chloro-2, 2, 2-trifuoroethyl-difluorormethylether; Isovet®, BRAUN, Rubi, Barcelona, Spain) diluted in 50 % O_2 and the experimenter was blinded to the genotype of mice. The scalp was incised along

the midline, and one hole was made at the appropriate stereotaxic coordinates from Bregma (mediolateral, 1 mm; anteroposterior, 2 mm; dorsoventral, 1.8 mm). 2 μL of 0.02 % red Fluorescent 2 μm microspheres in PBS was intracranial administrated (i.c.) at a rate of ≈0.5 μL/min.

Brain sections were stained with a rabbit polyclonal anti-Iba-1 (1:200) and revealed with goat anti-rabbit IgG labelled with Alexa 488 (1:400) obtained from Molecular Probes. For each coverslip, 4 random pictures were taken, using the TCS SPE confocal microscope (Leica Microsystems, Wetzlar, Germany). Images were analysed using ImageJ software (US National Institutes of Health, Bethesda, MD, United States). The number of fluorescent beads inside each cell was counted, and the average number of phagocyted microspheres per microglial cell was calculated for each experiment and treatment. Experiments were repeated at least 3 times for each condition.

2.9. Tissue processing for immunohistochemistry and immunofluorescence

2.9.1. Mouse brain

Mice were sacrificed by cervical dislocation and their forebrain removed. Brains were fixed in 4% paraformaldehyde and cryoprotected in 30 % sucrose solution. The samples were embedded in OCT compound (Sakura) and frozen using dry ice. Finally, 30 μm floating sections were cut in coronal planes with a cryostat (CM1950, Leica Microsystems) and stored in a solution of 30 % ethylene glycol, 30 % glycerol and 0.1 M PBS at −20 °C until processed.

2.9.2. Human brain

Whole brain from control, AD, and PiD subjects was separate into two hemispheres, through a sagittal interhemispheric incision, and fixed in 10 % buffered formalin for at least 3 weeks. Samples (2-mm-thick) of the hippocampus were then obtained through dissection, embedded in paraffin following standard protocols (Leica, HistoCore Pearl), and later sectioned (5 μm) by using a microtome (Microm HM 355 S) and stored at −80 °C until use.

2.10. Immunohistochemistry and immunofluorescence

2.10.1. For immunohistochemical analysis

Mouse sections were pre-treated for 45 min with 1 % H_2O_2 in PBS to inactivate endogenous peroxidase and then boiled in citrate buffer (citric acid 1 M in distillate H_2O) pH 5.9 for 5 min. Afterwards, sections were washed in PBS, blocked for 1 h. in block solution (1 % bovine serum albumin (BSA), Sigma-Aldrich, 5 % fetal bovine serum (FBS), and 0.2 % TritonX-100, Sigma-Aldrich, in PBS) and finally incubated ON at 4 °C with rabbit anti-P2X7 (1:100), rabbit anti-cleave caspase-3 (1:50), mouse anti-phospho tau (1:100). Later sections were incubated with avidin-biotin complex using the Elite Vectastain kit (Vector Laboratories, Burlingame, CA, USA) and chromogen reactions were performed with diaminobenzidine (DAB; Sigma-Aldrich) and 0.003 % H_2O_2 for 10 min.

2.10.2. For immunofluorescence studies

Mouse slices were boiled in citrate buffer, washed in PBS, blocked for 1 h at room temperature (RT) with blocking solution and then incubated at 37 °C for 1 h or overnight at 4 °C with primary antibodies diluted as follows: rabbit anti-P2X7 (1:100), chicken anti-GFP (1:500), mouse anti-GFAP (1:200), rabbit anti-Iba-1 (1:100), mouse anti-NeuN (1:100), rabbit anti Ki-67 (1:600) in blocking solution. Subsequently, brain sections were washed with PBS buffer and incubated with secondary antibodies at the following dilutions: anti-chicken IgG labelled with Alexa 488 (1:400), anti-rabbit IgG labelled with Alexa 555 (1:400), anti-rabbit IgG labelled with Alexa 488 (1:400), anti-mouse IgG labelled with Alexa 555 (1:400) and 4′,6-diamidino-2-phenylindole (DAPI) staining (1:1,000). Finally, brain sections were washed with PBS and mounted in FluorSave (Calbiochem).

2.10.3. For immunohistochemical and immunofluorescence studies

Human sections were pre-incubated at 55 °C ON and then sequentially washed for 10 min in Xylene (catalog 131769.1611, Panreac), ethanol 100 %, ethanol 96 %, ethanol 70 % and finally distilled H_2O in order to remove paraffin and rehydrated them. Later, the same protocols described for mouse samples were followed.

2.11. Image acquisition

Confocal images were acquired at RT with a TCS SPE microscope from Leica Microsystems equipped with a Plan Fluor 10× dry objective lens NA = 0.30, 40× Apochromat NA = 1.15 oil objective lens and 63× Apochromat NA = 1.3 oil objective lens (Leica Microsystems GmbH) and 4 different lasers lines (405, 488, 565 and 647 nm). Pictures were acquired using the Leica software LAS AF v2.2.1 software (Leica Microsystems GmbH) and representative slices converted to TIFF files using ImageJ software.

Transmitted light images were acquired using a microscope (DM 1000, Leica) with DFC450 CCD camera (Leica Microsystems GmbH) using Leica Application Suite (v4.1). Sections were photographed with Plan 4× dry objective lens (NA = 0.1) and insets with Plan S-Fluor 20× or 40× dry objective lens (NA = 0.90, Nikon) at RT.

2.12. Analysis of microglial morphology

Brain sections were stained with a rabbit polyclonal anti-Iba-1 (Wako 1:200) and revealed with goat anti-rabbit IgG labelled with Alexa 488 (1:400) obtained from Molecular Probes. For each slice, 4 random pictures were taken, using the TCS SPE confocal microscope (Leica Microsystems, Wetzlar, Germany). Images were analysed using FIJI software (US National Institutes of Health, Bethesda, MD, United States).

Skeleton analysis binary images were obtained from z-stack acquisition using a 40× objective. Binary images were then skeletonized and analysed through FIJI AnalyzeSkeleton (2D/3D) plugin, as previously described (Young and Morrison, 2018). The number of cell ramifications and the branch length were calculated for each experiment and treatment (at least 4 animals for experimental condition, each dot in the graphs represents the average of a minimum of 12 microglia cells).

For fractal analysis at least 18 random microglia cells from each experimental condition were analysed using FracLAc FIJI plugin. The area covered by cells was calculated for each experiment and treatment.

2.13. Tissue processing for Western blot

2.13.1. Mouse samples

Extracts for Western blot analysis were prepared by homogenizing fresh dissected mouse hippocampal area in ice-cold extraction buffer containing 20 mM Hepes, 100 mM NaCl, 50 mM NaF, 5 mM EDTA, 5 mM Na_3VO_4 (all from Sigma-Aldrich), 1 % Triton X-100, okadaic acid (Calbiochem), and Complete TM Protease Inhibitor Cocktail Tablets (Roche Diagnostics GmbH), pH 7.4. The samples were homogenized at 4 °C, and protein content was determined by Bradford assay

2.13.2. Human samples

Fresh samples of the hippocampus were obtained at the time of the autopsy, and they were immediately frozen in dry ice and stored at −80 °C for biochemical studies. Control, AD and PiD brain samples were processed following the same protocol as described for mouse samples.

2.14. Western blot analysis

Total protein (20 μg) from mouse or human samples was electrophoresed on 10 % Tris-Glycine-SDS gels and transferred to nitrocellulose membranes (Amersham Biosciences). The experiments were performed using the following primary antibodies: rabbit anti-P2X7 (1:1,000), mouse anti-α-Tubuline (1:10,000), mouse anti-AT8 (1:500), mouse anti-

TAU1 (1:500), mouse anti-PHF1 (1:1,000), mouse anti-TAU5 (1:10,000), rabbit anti-phospho-GSK-3 (pS21/9) (1:1,000), mouse anti-GSK3 α/β (1:1,000), rat anti-IL-1β (1:200), mouse anti-IL10 (1:200), mouse anti-IL6 (1:500), anti-GAPDH (1:20,000), rabbit anti-TNFα (1:500), mouse anti-β-actin (1:10,000), rabbit anti-TNAP (1:10,000), mouse anti-connexin 43 (1:100). The membranes were washed for 10 min with PBS-Tween three times and incubated with secondary antibodies for 1 h at room temperature. Secondary antibodies used were goat anti-mouse (1:1,000; 1:10,000) or goat anti-rabbit (1:1,000) or goat anti-rat (1:1,000) to horseradish peroxidase (HRP, Amersham GE Healthcare) followed by enhanced chemo luminescence detection (PerkinElmer, Waltham, MA, USA). Protein expression was standardized by the expression of α-Tubulin, β-actin, GAPDH, TAU5, or GSK3 from the same experiment. For CSF samples, total protein levels detected by Ponceau staining were used for normalization purpose (Collins et al., 2015).

Gel band images were captured with ImageQuant LAS 500 (GE Healthcare Life Sciences) and analyzed using ImageJ software (v1.52n, NIH, Bethesda, MD, United States). In the figures, the representative Western blot images show only the quantified bands.

2.15. ATPase activity

It was visualized as previously described (Sebastian-Serrano *et al.*, 2018b). Briefly, hippocampal sections from adult P301S or WT mice were washed in PBS and pre-treated with TMS (0.25 M sucrose, 50 mM Tris-maleate, 2 mM $MgCl_2$, pH 7.4) for 30 min at RT. The enzymatic reaction was carried out in TMS-buffered substrate solution stabilized with 3 % dextran T 40 (Roth) [TMS-S; 2 mM $Pb(NO_3)_2$, 5 mM $MnCl_2$, 2 mM $MgCl_2$, 50 mM Tris-maleate, pH 7.4, plus 0.25 M sucrose] containing the substrate 1 mM ATP (Sigma-Aldrich) for 90 min at 37 °C. The lead the dark orthophosphate precipitated, as a result of nucleotidase activity, was visualized as a brown deposit after to incubate sections for 1 min in an aqueous solution of $(NH_4)_2S$ (1 % v/v) (Sigma-Aldrich). Subsequently, sections were washed twice with PBS and mounted on glass slides with an anti-fading solution. To quantify the enzymatic reaction, we measured the amount of orthophosphate precipitate deposited on the hippocampus of WT and P301S mice. Values correspond to the mean intensity value of the pixel in eight bytes images containing the hippocampus (0–255 scale with 0 = white and 255 = black).

2.16. Statistics

Data are shown as mean values ± SEM. The numbers of mice per group used in each experiment are annotated as "n" in the corresponding figure legends. Figures and statistical analyses were generated using GraphPad Prism (v6.00, www.graphpad.com). To assess whether the data met the normal distribution, the Shapiro-Wilk or Kolmogorov-Smirnov tests were used. For two-group comparison, data were analysed with two-tailed unpaired Student's t test. For multiple comparisons, when only one variable was compared data were analysed by one-way ANOVA followed by Tukey's post hoc test, but when we analysed two independent variables, a two-way ANOVA followed by Tukey's post hoc test was used. The statistical test used, and p-values are indicated in each figure legend. Significance was considered at $*P \leqq 0.05$, $**P \leqq 0.01$, $***P \leqq 0.001$ or $****P \leqq 0.0001$ throughout the study.

3. Results

3.1. Microglial P2X7 is upregulated in Tauopathy patients and in the P301S mouse model

To confirm that the P2X7 upregulation found in AD patients is a common factor in Tauopathies, we analysed the expression levels of this receptor in post-mortem human hippocampal samples from two different Tauopathies, PiD and AD. We focused on this specific brain area because it is one of the most affected in Tauopathies. Results revealed that PiD patients show an increase in P2X7 protein levels similar to those observed in AD patients (227.5 ± 40.1 % for PiD patients and 190.2 ± 19.6 % for AD patients, Fig. 1A-B, supplementary Fig. 1A). A similar rise of *P2RX7* transcript levels was found in post-mortem hippocampal samples of PiD and AD as well (152.0 ± 8.7 % and 153.4 ± 1.3 % in PiD in AD respectively, Fig. 1C). Later immunohistological studies revealed that P2X7 positive cells mainly present a neuronal-like morphology in the hippocampus of healthy controls, observing a lower incidence in hippocampi from AD and PiD patients (Fig. 1D). Considering that previous studies have reported an enrichment of microglial cells expressing P2X7 in AD patients (Martin et al., 2019; Martinez-Frailes et al., 2019; McLarnon et al., 2006; Parvathenani et al., 2003), initially we co-stained the hippocampal post-mortem samples from Tauopathy patients with the antibodies anti-P2X7 and anti-Iba-1 (a specific microglial marker). Our results showed that PiD and AD patients presented a higher incidence of hippocampal microglial cells expressing P2X7 than the healthy controls (specifically 2-fold increase in P2X7 positive microglial cells in AD patients and 2.5-fold increase in PiD patients, Fig. 1E). Further studies using the specific astroglia marker GFAP revealed that AD and PiD patients also show an enrichment in hippocampal astrocytes expressing P2X7 (1.6-fold and 1.8-fold increase in astrocytes expressing P2X7 in AD and PiD patients respectively supplementary Fig. 1B).

Next, we investigated whether this condition was phenocopied in one of the most widely used mouse models of tauopathy, namely the P301S mouse (Yoshiyama et al., 2007). Our analysis revealed that hippocampi of 9-months-old heterozygous P301S mice (P301S) show an increase of 160.2 ± 3.2 % of P2X7 protein and 154.1 ± 0.2 % of *P2rx7* mRNA respect to protein and messenger levels detected in their WT littermates (Fig. 1F-H). Immunofluorescence studies confirmed that P301S mice present a higher incidence of microglial cells and astrocytes expressing P2X7 than WT mice (Fig. 1I and supplementary Fig. 1C). To confirm that glial P2X7 upregulation was the result of increased *P2rx7* gene transcription, we crossbred P301S mice with P2X7 reporter mice (^{P2X7}EGFP) that express soluble EGFP under the control of the P2X7 promoter (Sebastian-Serrano et al., 2016). Comparative analysis of cell-type specific expression by immunofluorescence demonstrated that ^{P2X7}EGFP;P301S mice presented a higher transcription of *P2rx7* gene in hippocampal glial linages, especially in microglial cells (three times more), than ^{P2X7}EGFP mice (supplementary Fig. 2B, D and E). Interestingly, although ^{P2X7}EGFP;P301S mice showed higher expression of P2X7 protein than their corresponding ^{P2X7}EGFP littermates (supplementary Fig. 2A), a significant reduction on *Prx7* gene transcription was found in neuronal cells (supplementary Fig. 2B and C).

Finally, to elucidate the activation degree of the upregulated P2X7Rs, we evaluated different parameters controlling the levels of its native ligand, extracellular ATP. Thus, we measured the hippocampal ATPase activity to assess the extracellular degradation capacity of ATP and hippocampal Connexin-43, a protein-related with the non-vesicular ATP release. Our results revealed that P301S mice presents lower hippocampal ATPase activity and higher expression of Connexin-43 than those observed in the hippocampus of their corresponding age-matched WT mice (supplementary Fig. 3A-D).

3.2. Pharmacological inhibition of P2X7 improves cognitive and motor deficiencies associated with P301S mice

To study the effect of P2X7 upregulation on Tau-induced toxicity, we analysed whether *in vivo* pharmacological inhibition of this receptor affects the characteristic behavioural alterations of P301S mice. To this aim, a set of 9 months old P301S and WT mice were treated daily with the blood-brain barrier permeable selective P2X7 antagonist GSK 1482160A (GSK, 100 mg/kg, i.p) (Martinez-Frailes et al., 2019; Territo et al., 2017) or the same volume of vehicle solution (Veh) for 3 weeks (Fig. 2A). After the treatment, the cognitive status of the four generated groups was evaluated by a battery of behavioural tests. The anxiety-like

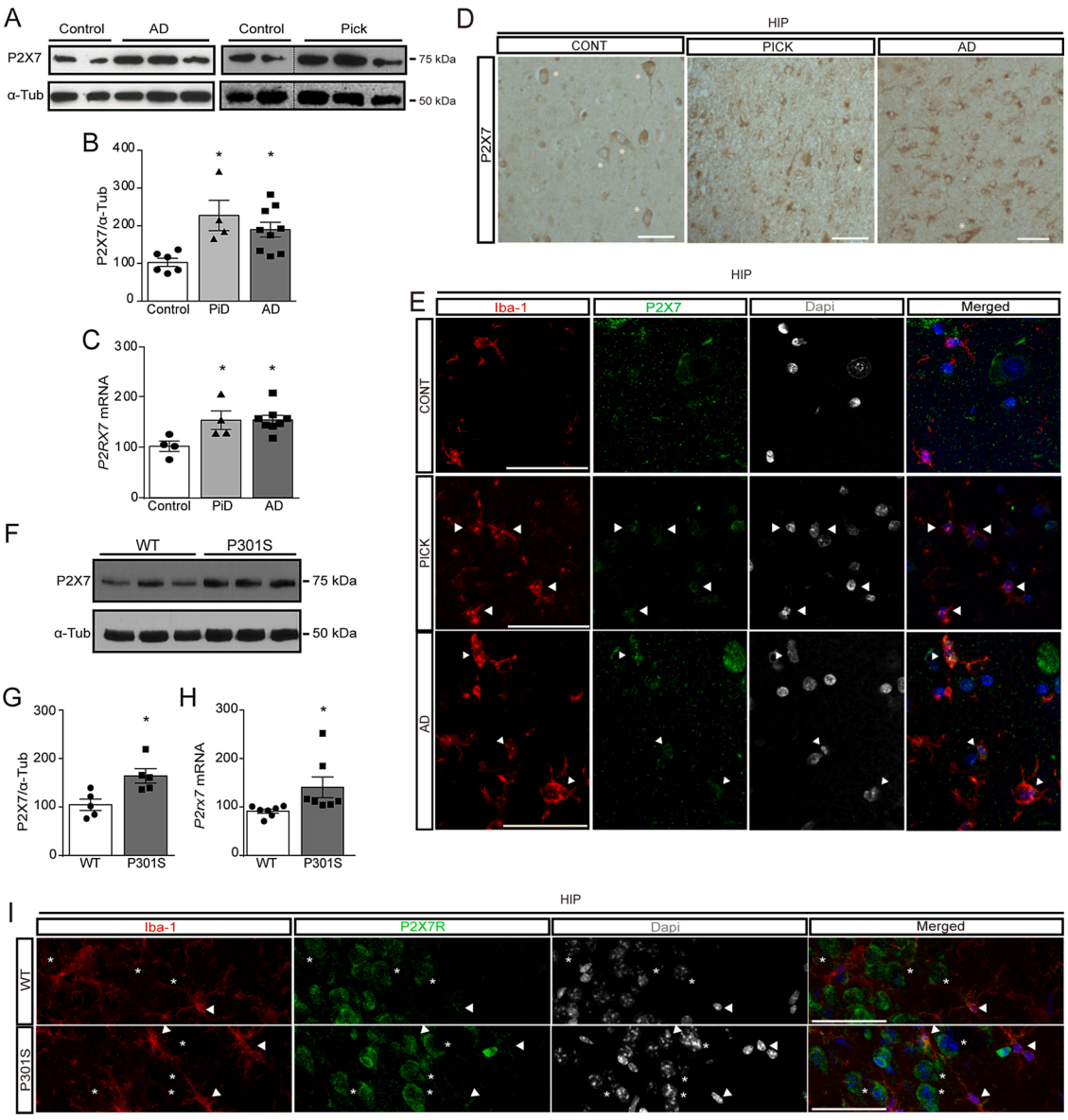

Fig. 1. Upregulation of P2Xx7 expression in microglia cells from AD and PiD diagnosed patients and in the P301S Tauopathy mouse model. (A), Representative immunoblots of P2X7 using homogenates from hippocampal necropsies from Alzheimer's disease (AD) or Pick's disease (PiD) patients and non-affected individuals (Control). (B), Quantification of P2X7 protein levels in homogenates from hippocampal necropsies from AD (n = 9) and PiD patients (n = 4) and non-affected individuals (n = 6). Levels of α-Tubulin (α-Tub) were used as loading control for normalization purposes. (C), Quantification of *P2RX7* mRNA in the hippocampus from human controls (n = 4), AD patients (n = 8) and PiD patients (n = 4). In all cases, the 100 % value corresponds to the averaged amount of protein or messenger of P2X7 detected in the hippocampi of non-affected individuals. * $P \leqq 0.05$ using a One-way ANOVA followed by Tukey's post hoc test. (D) Representative images of immunohistochemical staining for P2X7 in hippocampi from human controls, AD and PiD patients. Asterisks point to brain cells showing neuronal-like morphology. Scale bar = 50 μm. (E) Hippocampal sections from human controls, AD and PiD patients stained with specific microglial marker (Iba-1, red channel), P2X7 (green channel) and DAPI (grey channel). Merged images showing DAPI channel in blue are also showed. Arrowheads indicate microglial cells expressing P2X7. Scale bar: 50 μm. (F) Representative immunoblot of P2X7 protein levels in homogenates from hippocampi of 9-month-old P301S and wild-type (WT) mice of the same age. α-Tub was used as loading control. (G) Graph show P2X7 proteins levels in P301S and WT mice (n = 5 mice per genotype). (H) Quantification of *P2rx7* mRNA in the hippocampus from P301S (n = 7) and WT (n = 7) mice. (I) Parasagittal sections of hippocampus from P301S and WT mice stained with specific microglial marker (Iba-1, red channel), P2X7 (green channel) and DAPI (grey channel). Merged images showing DAPI channel in blue are also showed. Arrowheads indicate microglial cells expressing P2X7 and asterisks indicate P2X7 positive cells that are not microglia. Scale bar: 50 μm. Data represent the mean ± standard error (SEM). * $P \leqq 0.05$ using unpaired two tailed Student's *t*-test.

behaviour of P301S mice was evaluated in the open field test (OF). Our analysis revealed that vehicle-treated P301S (Veh-P301S) mice spent more time in the central area than their vehicle-treated WT littermates (Veh-WT) but did not present significant differences in the total distance travelled (Fig. 2B). The decreased anxiety-like behaviour was confirmed in the more specific elevated-plus maze test (EPM) (Supplementary Fig. 4A). Interestingly, the P2X7 antagonist treatment prevented this reduction in P301S mice (Fig. 2B). The motor coordination of P301S mice was assessed using the rotarod apparatus. As shown in Fig. 2C, Veh-P301S mice exhibited a deteriorated motor performance. On the contrary, GSK-P301S mice showed a similar motor coordination to Veh- or GSK-WT mice (Fig. 2C). Finally, at the tested age, P301S mice began to show a tendency to reduced memory capacity, which was detectable by the novel object recognition test (NOR) (Fig. 2D). Interestingly, pharmacological blockade of P2X7 not only prevented this trend but significantly improved the memory capacity of P301S mice (Fig. 2D). All

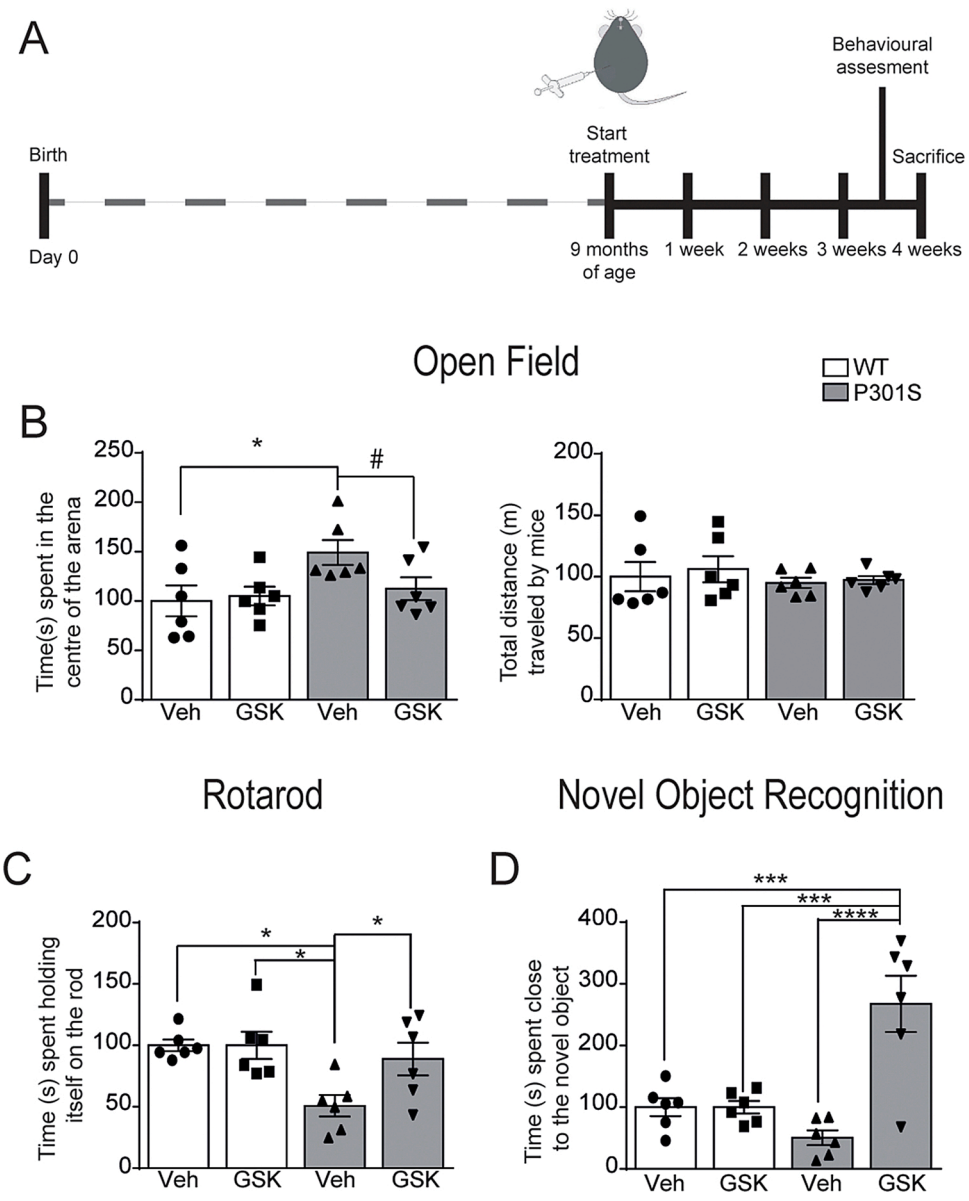

Fig. 2. *In vivo* pharmacological blockage of P2X7 rescues some of the behavioural deficits associated with Tauopathies in P301S mice. (A) Schematic timeline of the experimental schedule. WT and P301S mice were intraperitoneally treated with either a vehicle solution or with the P2X7 antagonist GSK 1482160A (GSK) for 3 weeks. At the end of the treatment all mice (Veh-WT n = 6, GSK-WT n = 6, Veh-P301S n = 6, GSK-P301S n = 6) underwent the open field test (OF), the rotarod test (RT), and the novel object test (NOR) paradigms. (B) OF; graphs represent the time(s) spent by the mice in the centre of the arena (left graph) and the total distance travelled by mice in the apparatus (right graph). (C) RT; graph represents the time (s) spent by the mice holding on the rod before falling dawn. (D) NOR; graph represents the time(s) that the mice spent exploring the new object. Data represent the mean ± standard error (SEM). * $P \leqq 0.05$; *** $P \leqq 0.001$; **** $P \leqq 0.0001$ using a two-way ANOVA followed by Tukey's post hoc test. # $P \leqq 0.05$ using unpaired two tailed Student's *t*-test.

these data indicate that P2X7 antagonists improve anxiety-related and memory deficits as well as motor coordination in P301S mice.

3.3. *In vivo P2X7 blockade affects the microglial functionality*

After behavioural assessment, the mice were sacrificed and analysed to assess the impact of P2X7 inhibition on Tauopathy. We initially focused on the effects of P2X7 blockade on microglia. Therefore, microglial properties including phagocytic, migratory, secretory and proliferation capacities, were analysed. Microglia proliferation was initially evaluated by counting the number of hippocampal microglia cells identified by the microglial marker Iba-1. As shown in Fig. 3A, Veh-P301S mice presented a significant higher number of hippocampal microglia cells than Veh-WT mice (475.5 ± 38.8 in Veh-P301S mice *vs* 290.8 ± 22.0 in Veh-WT mice). Increased microglial proliferation rate in P301S mice was confirmed using the proliferation marker Ki-67 (Veh-P301S mice showed 51.4 ± 8.3 % more Iba-1 and Ki-67 positive cells than Veh-WT, supplementary Fig. 4B-C). Interestingly GSK-P301S mice presented a similar number of both hippocampal microglia cells and Ki-67 positive microglial cells as Veh-WT mice or GSK-WT mice (Fig. 3A and supplementary Fig. 4B-C). Conversely, pharmacological P2X7 blockage did not modify the increased astroglial proliferation rate found in P301S mice (supplementary Fig. 4D-E)

To estimate microglial phagocytic capacity, five micron-diameter fluorescent microspheres were intrahippocampally (i.h.) administered to a new set of WT and P301S mice. 8 days before the injection the mice were treated with GSK 1482160A or vehicle solution every 24 h. Three days after microsphere injection, mice were sacrificed, and hippocampal sections were stained with anti-Iba-1 antibody to identify microglia cells (Fig. 3B). Importantly, although we did not detect an enrichment of microglia cells phagocytosing microspheres in the analyzed groups (Fig. 3B and C), P2X7 blockade caused a significant increase in microglial phagocytic capacity in both WT and P301S mice (1.4 ± 0.2 and 1.6 ± 0.3 phagocyted beads per microglia in Veh-WT and Veh-P301S mice respectively *versus* 2.5 ± 0.4 and 3.0 ± 0.6 phagocyted beads per microglia in GSK-WT and GSK-P301S mice respectively Fig. 3B-D).

We next evaluated the microglial migration capacity analysing the injection-induced microglial recruitment to the injury site *in vivo* (Fig. 3E). The results revealed that P2X7 inhibition reduced the number of microglia at the injection injury site in P301S mice, observing a similar tendency in WT mice (Fig. 3E).

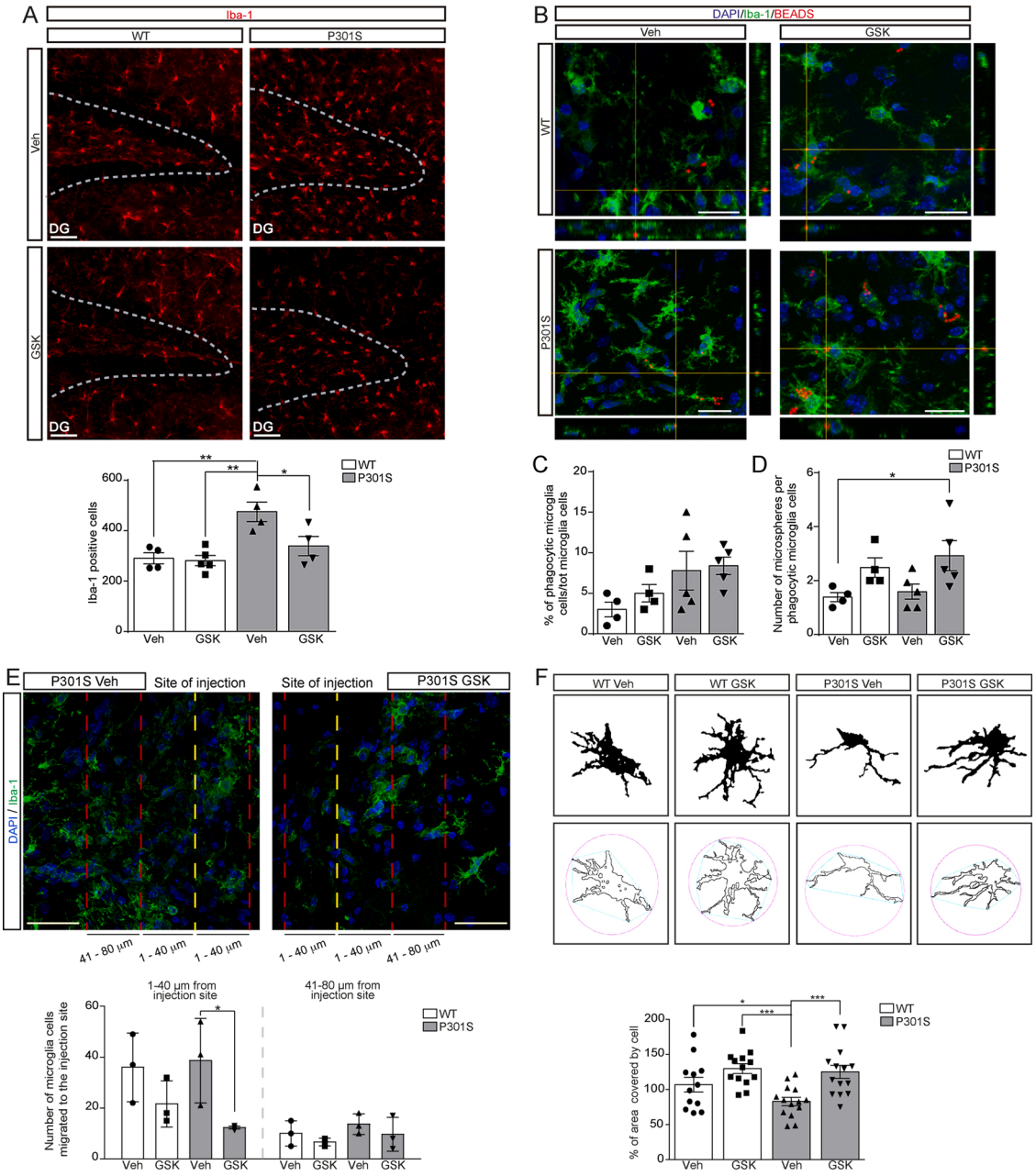

Fig. 3. Pharmacological P2X7 blockade reverts microglial proliferation, secretion, and migration caused by Tau-induced toxicity and promotes microglial phagocytosis. (A) Representative images of hippocampal sections from P301S and WT mice treated with vehicle solution or the P2X7 antagonist GSK 1482160A (GSK), 100 mg/kg, i.p) stained with the microglial marker Iba-1. Dash lines indicates the granular layer of the dentate gyrus (DG). Scale bar: 100 µm. The graph represents the quantification of Iba-1 positive cells in the hippocampus (n≧4 mice per genotype and treatment with n≧4 sections/mouse). (B) Representative confocal images and its corresponding orthogonal views of hippocampal sections from 9 months-old WT and P301S mice intraperitoneally treated with either vehicle solution or GSK for 3 weeks before intracranial administration of fluorescent microspheres to the hippocampus. Yellow lines represent the location where an orthogonal view was obtained. Sections were stained with antibodies against microglial marker Iba-1 (green) and nuclear marker DAPI (blue). Fluorescent microspheres are visualized in red. Scale bar: 25 µm. Graphs represent the % of microglial cells taking up microspheres (C) and the number of incorporated fluorescent microspheres per microglia (D) (n≧4 mice per genotype and treatment and, n ≧4 sections per mouse). (E) Representative immunofluorescence images of hippocampal sections stained with microglial marker Iba-1 used to evaluate the microglial migration toward the site of injection (yellow line). Distances of 40 and 80 µm from the injured site are identified with dash red lines. The graph represents the number of hippocampal microglial cells found in every delimitated area (n≧3 mice per genotype and treatment and, n≧4 sections per mouse). (F) Representative images showing the binary image of microglia cells (upper panels) with their corresponding outline and associated convex hull (blue) and enclosing circle (pink) for the corresponding outline shapes (bottom panels). Graphs show the percentage of brain area covered by microglia cells for each condition. The 100 % value corresponds to the brain area covered by microglia cells in WT mice (n = 10 random microglia cells per genotype and experimental condition). Data represent the mean ± standard error (SEM). * $P \leqq 0.05$; ** $P \leqq 0.01$; *** $P \leqq 0.001$ using a two-way ANOVA followed by Tukey's post hoc test.

To evaluate the microglial secretion, we analysed hippocampal levels of different cytokines. As expected, Veh-P301S mice showed higher levels of IL-1β (49.6 ± 11.7 % more, supplementary Fig. 4F-G) and IL-6 (158.6 ± 35.3 % more, supplementary Fig. 4F and H) than Veh-WT mice. Additionally, a non-significant difference in hippocampal TNF-α levels was detected (Supplementary Fig. 4F and I). P2X7 blockade reverted the increased in IL-1β levels but did not affect the elevated IL-6 levels detected in P301S mice (supplementary Fig. 4F-H). Remarkably, pharmacological inhibition of P2X7R did not significantly modify the levels of the analyzed cytokines in WT mice (supplementary Fig. 4F-I).

Given that P2X7 was shown to promote elongation and branching of neuronal processes (Diaz-Hernandez et al., 2008), we also assessed the impact of P2X7 pharmacological blockade on microglial morphology. Our analysis revealed that Veh-P301S mice present less ramified hippocampal microglia than Veh-WT mice and thus cover less hippocampal area in Veh-P301S mice than in Veh-WT mice (Fig. 3F and supplementary Fig. 5). It is to note that the *in vivo* P2X7 blockage reverted these differences, indeed, the GSK-P301S mice showed hippocampal microglial cells with a similar number of ramifications and length than those observed in Veh-WT mice, thus enabling them to cover a similar hippocampal area as in WT mice (Fig. 3F and supplementary Fig. 5). To confirm the critical role that P2X7 seems to have on microglia, we evaluated the effect of its genetic overexpression. To this end, we compared the microglia cell morphology in a BAC transgenic mouse line overexpressing an P2X7 receptor fused to EGFP (P2X7^{451P}EGFP) (Kaczmarek-Hajek et al., 2018) and their WT littermates. Remarkably, P2X7 overexpressing microglia cells presented shorter processes, smaller cellular size and nuclei area than WT microglia, and consequently covered a smaller hippocampal area (supplementary Fig. 6A-E).

Altogether, the functional and morphological changes observed in microglial cells from P301S mice support the hypothesis that these cells are in an activated state and that the blockade of P2X7 reverts this state. Moreover, our results are indicating that P2X7 overexpression is sufficient to cause the morphological changes associated with microglial activation.

3.4. Pharmacological P2X7 blockade reverts cellular death, reduces intracellular Tau phosphorylation and promotes extracellular Tau (eTau) phosphorylation in vivo

Since previous studies reported that P2X7 inhibition reduces neuronal death associated with different neurodegenerative diseases, including Huntington disease (HD) and AD (Diaz-Hernandez et al., 2012, 2009), we decided to elucidate if P2X7 inhibition generally improves neuronal survival in Tauopathies. Our studies revealed that Veh-P301S mice present a significant reduction of hippocampal neurons compared to Veh-WT mice (38.3 ± 2.2 % less than Veh-WT mice, Fig. 4A). Accordingly, Veh-P301S mice showed a higher number of hippocampal cleaved-Caspase-3 positive apoptotic cells than Veh-WT mice (5.4 ± 2.4 times more than Veh-WT mice, Fig. 4B). However, P2X7 antagonist-treated GSK-P301S mice neither showed the reduction in hippocampal neurons nor the increase in apoptotic cells detected in Veh-P301S mice (Fig. 4A-B).

As it was reported that pharmacological inhibition of P2X7 reduced the intraneuronal Tau phosphorylation *via* glycogen synthase kinase-3 (GSK3) in cultured hippocampal neurons (Diaz-Hernandez et al., 2008), we next analyzed the status of different intracellular Tau phosphorylation sites related to Tau-induced toxicity. P2X7 blockade significantly reduced the phosphorylation rate of Tau protein in Ser202/Thr305 sites and Ser 396/404, detectable by AT8 and PHF1 antibodies respectively (50.1 ± 1.7 % and 27.2 ± 12.3 % lower than in Veh-P301S mice respectively, Fig. 4C-E). In agreement with these results, a significantly increased dephosphorylation was detected in Ser 195/198/199/202 with TAU1 antibody (72.3 ± 20.4 % higher than in Veh-P301S mice, Fig. 4C and F). Noteworthy, later immunodetection studies confirmed that P2X7 inhibition caused a significant reduction in the number of positive AT8 stained neurons (Fig. 4G-H). Supporting the importance that P2X7 plays in regulating the phosphorylation rate of intraneuronal Tau protein, we found that mice overexpressing P2X7 (P2X7^{451P}EGFP) have significantly higher levels of phosphorylated Ser202 and Thr205 sites than their corresponding WT littermate mice (Supplementary Fig. 6F-G). But they showed neither an alteration in the total amount of Tau protein nor a significant neuronal loss (Supplementary Fig. 6F-J). Remarkably, we also found that P301S mice presented a lower phosphorylated rate of GSK3 in Ser 9/21 sites than WT mice (25.2 ± 1.5 % minor, Fig. 4I-K). It is to note that the i.p. administration of GSK 1482160A raised the phosphorylation rate of GSK3 in the indicated serine residues (89.4 ± 14.2 % higher than in Veh-P301S mice Fig. 4L-N). Since phosphorylation of Ser 9/21 sites in GSK3 has been related to a decreased GSK3 enzyme activity (Diaz-Hernandez et al., 2012, 2008), we can hypothesize that P2X7-blockade promotes Tau dephosphorylation by inhibiting GSK3.

Furthermore, given that previous studies reported that extracellular Tau protein (eTau) dephosphorylated also contributes to Tau-induced toxicity (Diaz-Hernandez et al., 2010), we decided to measure the phosphorylated eTau levels in CSF collected from P301S mice treated or not with GSK 1482160A. Our results revealed that the P2X7 blockade raised the phosphorylated rate of eTau protein in Ser202/Thr205 sites (Fig. 4O). Considering these results, we analysed the levels of the tissue-nonspecific alkaline phosphatase (TNAP), an ectoenzyme that dephosphorylates the eTau (Diaz-Hernandez et al., 2010). We found that P301S mice presented higher hippocampal TNAP levels than WT mice (supplementary Fig. 7A). Interestingly, *in vivo* pharmacological P2X7 blockage caused a significant reduction of hippocampal TNAP levels in P301S mice (Fig. 4L and P). Finally, to investigate if there was a causal relationship between Tau-induced neuroinflammation and the observed TNAP upregulation in the hippocampus of P301S mice, we analysed the expression levels of this ectoenzyme in the hippocampus of WT mice after LPS-induced neuroinflammation. Our results revealed that LPS-induced neuroinflammation causes a significant increase in hippocampal TNAP expression (supplementary Fig. 7B).

3.5. P2X7 knockout ameliorates Tau-induced toxicity whereas its overexpression aggravates it

To confirm the potential therapeutic role of P2X7 in Tauopathies, we evaluated how the genetic depletion or overexpression of P2X7 affects Tau-induced toxicity. To this end, P301S mice were crossbreed with P2X7 knock-out mice (P2X7$^{-/-}$) or with P2X7^{451P}EGFP mice (Kaczmarek-Hajek et al., 2018). These newly generated transgenic lines, P301S;P2X7$^{-/-}$ and P301S;P2X7^{451P}EGFP, were evaluated using a similar battery of behavioural tests than that used in the pharmacological approach. In agreement with the data from P2X7 antagonist-treated mice, P301S;P2X7$^{-/-}$ mice showed lower scores than the ones detected for P301S mice in EPM test (Supplementary Fig. 8A). Similarly, P301S;P2X7$^{-/-}$ mice spent more time than littermates P301S mice both in the rotarod apparatus and exploring the novel object in the NOR test (Fig. 5A-B). In contrast, P301S;P2X7^{451P}EGFP mice obtained opposite results in both tests (Fig. 5A-B) but they did not spend more time in the open arms in the EPM test than P301S mice (Supplementary Fig. 8A).

After their behavioural assessment, mice were sacrificed for biochemical analysis. Firstly, these analyses allowed to confirm both the absence of hippocampal P2X7 in P301S;P2X7$^{-/-}$ mice and P2X7 overexpression in P301S;P2X7^{451P}EGFP mice (supplementary Fig. 7C-D). In agreement with the pharmacological studies, the absence of P2X7 caused a significant rise of GSK3 phosphorylation (54.4 ± 7.6 % higher than P301S mice, Fig. 5C) and a reduction in the intracellular Tau phosphorylation rate in P301S mice (60.1 ± 15.2 % lower than P301S mice, Fig. 5D). Accordingly, a significant reduction in the number of positive AT8 stained neurons was observed in P301S;P2X7$^{-/-}$ mice as well (Fig. 5E-F). Interestingly, P301S;P2X7$^{-/-}$ mice presented a 38.4 ± 6.5 % more hippocampal neurons than in P301S mice (Fig. 5G-H).

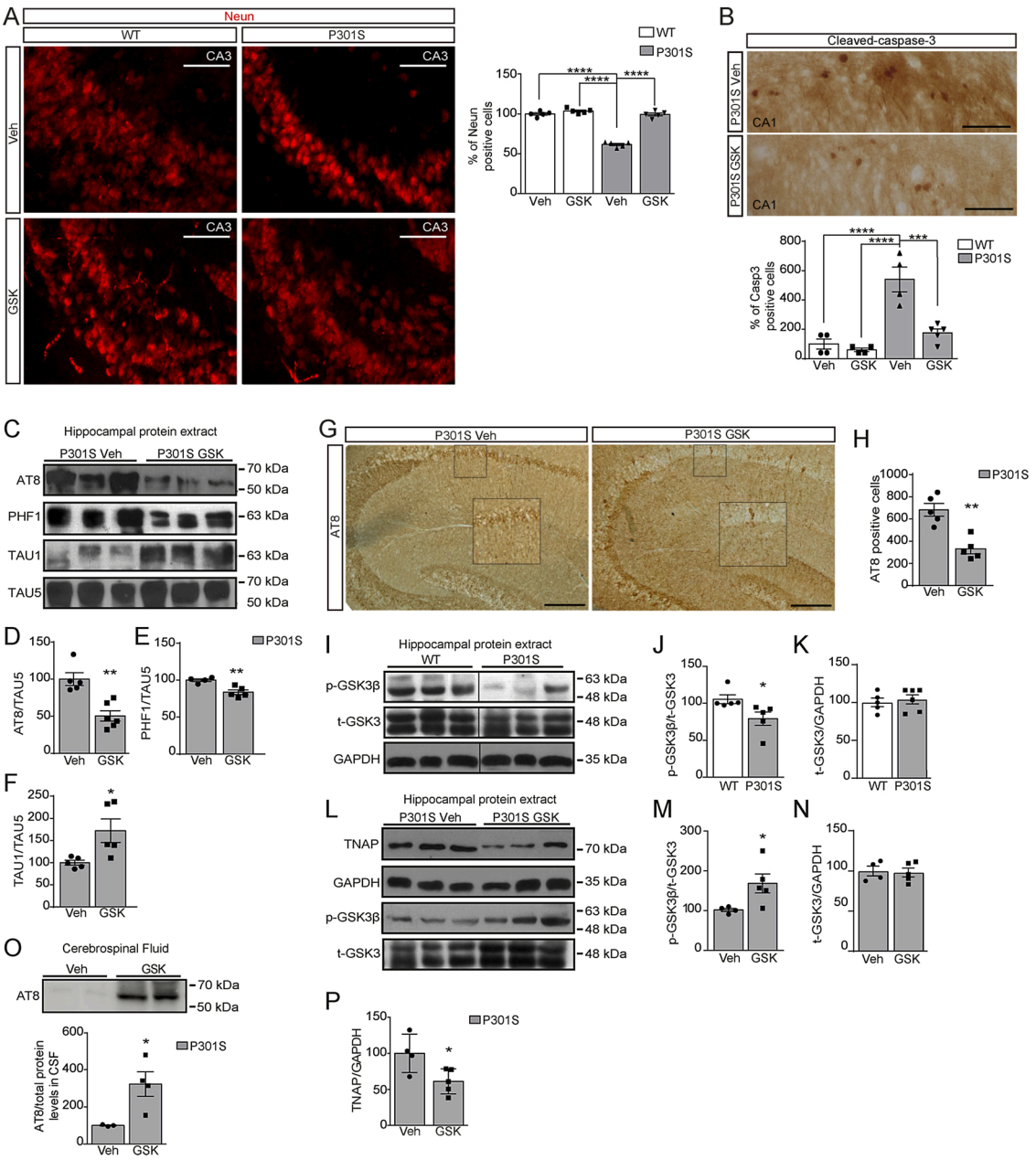

Fig. 4. *In vivo* P2X7 inhibition enhances neuronal survival by causing opposite effects in intra- and extracellular Tau proteins. (A) Representative immunofluorescence images of hippocampal CA3 area stained with NeuN from WT and P301S mice treated with vehicle solution or the P2X7 inhibitor GSK 1482160A (GSK, 100 mg/kg, i.p). Scale bar = 100 μm. Graph represents the quantification of neuronal hippocampal cells identified as NeuN positive (n≧4 mice per genotype and treatment and n≧4 sections per mouse). (B) Cleaved Caspase-3 immunostaining in hippocampus from WT and P301S mice treated with vehicle solution or GSK. Scale bar = 100 μm. Graph represents the quantification of hippocampal cleaved Caspase-3 positive cells (n≧4 mice per genotype and treatment and n≧4 sections per mouse). *** $P \leqq 0.001$; **** $P \leqq 0.0001$ using a two-way ANOVA followed by Tukey's post hoc test. (C) Western blot detection of the different Tau phosphorylation sites in hippocampal protein extract. Graphs show the quantification of phosphorylated Tau protein levels identified by the selective antibodies AT8 (D), PHF-1(E), TAU1 (F) in homogenates of hippocampus from P301S mice treated with vehicle solution (n = 5-4 mice) or P2X7 inhibitor GSK (n = 6-5 mice). Total Tau protein levels were identified using the antibody Tau5 and were used as a loading control for normalization purposes. The 100 % value corresponds to the amount of phosphorylated Tau levels detected in the hippocampi of vehicle treated P301S mice. (G)AT8 immunostaining in hippocampus from P301S mice treated with vehicle solution or GSK. Insert represent a x2 magnification of the indicated area. Scale bars = 100 μm. (H) Graph represents the quantification of AT8 positive cells both in Veh-P301S and GSK- P301S mice (n≧4 mice per genotype and treatment and n≧4 sections per mouse). ** $P \leqq 0.01$ using an unpaired two tailed Student's *t*-test. (I-K) Quantification of p-GSK3β levels in the hippocampus from WT and P301S mice (n = 5 mice per genotype), or (L-N) P301S mice treated with vehicle or GSK (n = 5 mice per treatment). Levels of total-GSK3 were used as loading control for normalization purposes. The 100 % value corresponds to p-GSK3β/t-GSK3 levels detected in the hippocampi of WT mice or vehicle treated P301S mice respectively. Data represent the mean ± standard error (SEM). * $P \leqq 0.05$; ** $P \leqq 0.01$ using an unpaired two tailed Student's *t*-test. (O) Representative immunoblot and quantification of phospho-Tau (Ser202/Thr205) protein levels in CSF samples from P301S mice treated with vehicle or GSK (n = 3 mice per genotype and treatment). Total protein level detected by ponceau staining were used as loading control for normalization purposes. The 100 % value corresponds to phospho-Tau protein levels detected in CSF from vehicle treated P301S mice. (P) Graph shows the quantification of TNAP levels detected both in Veh-P301S and GSK-P301S mice. The 100 % value corresponds to TNAP levels detected in Veh-treated P301S mice. * $P \leqq 0.05$ using an unpaired two tailed Student's *t*-test.

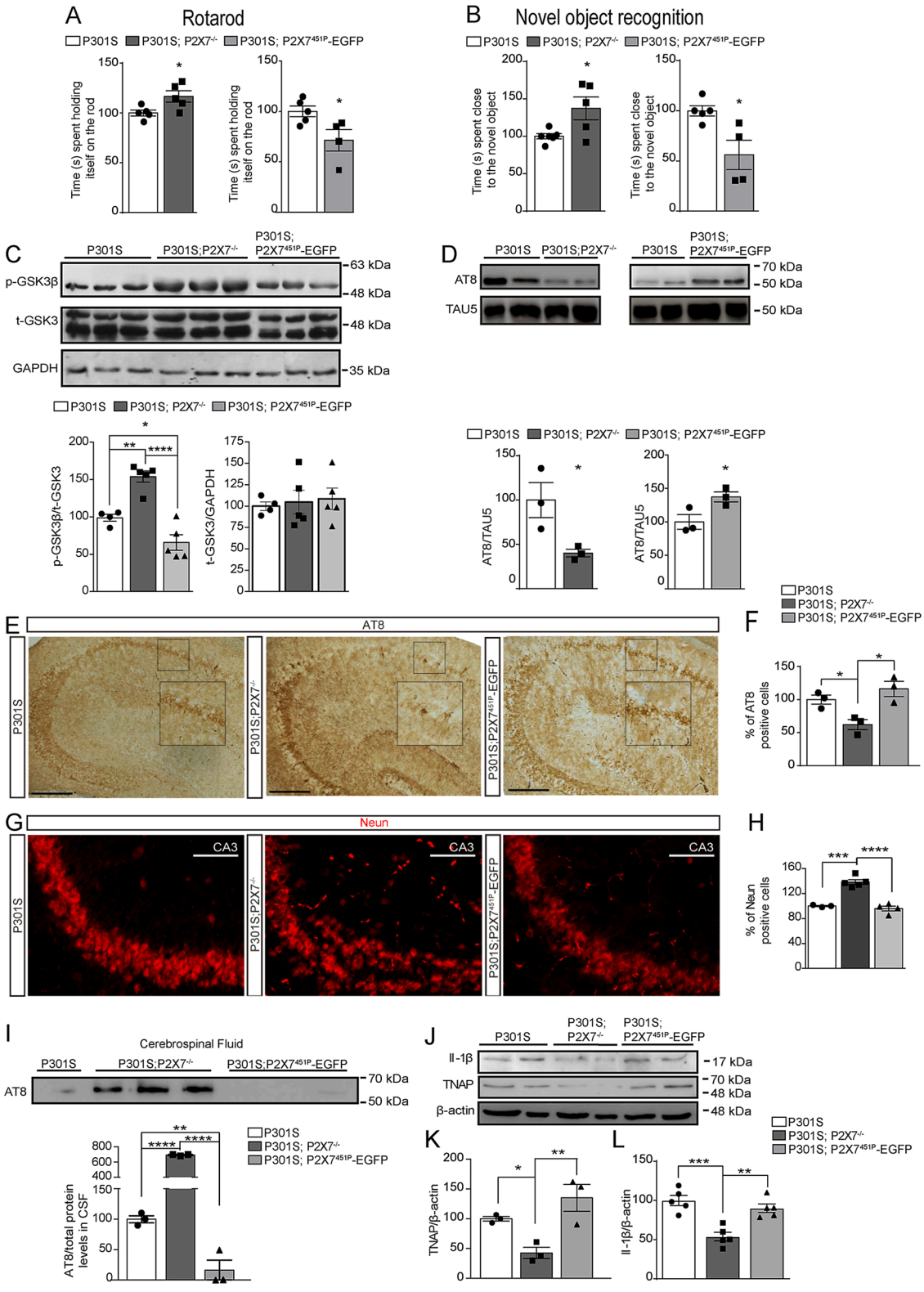

(caption on next page)

Fig. 5. Genetic P2X7 knockdown rescues behavioural deficits associated with Tauopathies in P301S mice whereas its overexpression worsens them. (A) 6 months-old P301S, P301S;P2X7$^{-/-}$, and P301S;P2X7^{451P}-EGFP mice underwent the rotarod test (RT) and the novel object test (NOR). (A) RT; graph represents the time(s) spent by the mice holding on the rod before falling dawn. (B) NOR; graph represents the time(s) that mice spent exploring the new object. Data represent the mean ± standard error (SEM) (n = 4 P301S;P2X7^{451P}-EGFP mice, n = 6 P301S;P2X7$^{-/-}$mice and n = 6-4 P301S mice). * $P \leqq 0.05$ using unpaired two tailed Student's *t*-test. (C) Representative immunoblots and quantification of p-GSK3 and total GSK3 (tGSK3) protein levels in hippocampal homogenates from P301S, P301S;P2X7$^{-/-}$, and P301S;P2X7^{451P}-EGFP mice (n = 5-3 mice per genotype). Levels of tGSK3 and GAPDH were used as loading control for normalization purposes. The 100 % value corresponds to p-GSK3β/t-GSK3 or tGSK3/GAPDH levels detected in the hippocampi of P301S mice respectively. * $P \leqq 0.05$; ** $P \leqq 0.01$; **** $P \leqq 0.0001$ using a One-way ANOVA followed by Tukey's post hoc test. (D) Representative immunoblot and quantification of phosphorylated Tau protein levels in hippocampal homogenates from P301S, P301S;P2X7$^{-/-}$, and P301S;P2X7^{451P}-EGFP mice (n = 3 mice per genotype). Levels of total Tau proteins were used as loading control for normalization. The 100 % value corresponds to AT8/TAU5 levels detected in the hippocampi of P301S mice. * $P \leqq 0.05$ using an unpaired two tailed Student's *t*-test. (E) Representative images of hippocampal slices from P301S, P301S;P2X7$^{-/-}$, and P301S;P2X7^{451P}-EGFP mice stained with antibodies anti phospho-Tau (AT8, n = 3 mice per genotype and n≥4 sections per mouse). Scale bars: 100 μm. Insert represent a x2 magnification of the indicated area. (F) Graph represents the quantification of AT8 positive cells. * $P \leqq 0.05$ using a One-way ANOVA followed by Tukey's post hoc test. (G) Representative images of hippocampal CA3 area slices from P301S, P301S;P2X7$^{-/-}$, and P301S;P2X7^{451P}-EGFP mice stained with NeuN (n = 3-5 mice per genotype and n≥4 sections per mouse). Scale bars: 100 μm. (H) Graph represents the quantification of NeuN positive cells. *** $P \leqq 0.001$; **** $P \leqq 0.0001$ using a One-way ANOVA followed by Tukey's post hoc test. (I) Representative immunoblot and quantification of phospho-Tau (Ser202/Thr205) protein levels in CSF samples from P301S, P301S;P2X7$^{-/-}$, and P301S;P2X7^{451P}-EGFP mice (n = 3 mice per genotype). Total protein level detected by ponceau staining were used as loading control for normalization purposes. The 100 % value corresponds to phospho-Tau protein levels detected in CSF from P301S mice. ** $P \leqq 0.01$; **** $P \leqq 0.0001$ using a One-way ANOVA followed by Tukey's post hoc test. (J) Western blot detection of IL-1β and TNAP levels in hippocampal protein extract from P301S, P301S;P2X7$^{-/-}$, and P301S;P2X7^{451P}-EGFP mice (n = 3 mice per genotype). Graphs show the quantification of TNAP (K) and IL-1β (L) levels in homogenates of hippocampus from P301S, P301S;P2X7$^{-/-}$, and P301S;P2X7^{451P}-EGFP mice (n = 3-5 mice per genotype). Total β-actin protein levels were used as a loading control for normalization purposes. The 100 % value corresponds to the amount of TNAP (K) and IL-1β (L) levels detected in the hippocampi of P301S mice. * $P \leqq 0.05$; ** $P \leqq 0.01$; *** $P \leqq 0.001$ using a One-way ANOVA followed Tukey's post hoc test.

Furthermore, P301S;P2X7$^{-/-}$ mice presented significantly lower TNAP levels and higher phosphorylated eTau levels than P301S mice (Fig. 5I-K). Finally, we observed that P301S;P2X7$^{-/-}$ mice secreted less IL-1β than the P301S mice (Fig. 5J and L). In good agreement, we observed that P301S;P2X7-/- mice showed lower number of hippocampal microglial cells than P301S mice, but no differences were found in the number of astrocytes (supplementary Fig. 8B-C, and H–I). Moreover, microglial cells from P301S;P2X7-/- mice showed a higher number of more extended ramifications than P301S mice leading them to cover a wider hippocampal area (supplementary Fig. 8D-G). Altogether, the above data indicate that genetic P2X7 knockout results in i) a reduced phosphorylation rate of intraneuronal Tau protein in a GSK3 dependent way, ii) a rise of phosphorylated eTau by decreasing TNAP expression and iii) reverts the microglial activation.

On the other hand, P2X7 overexpression caused a significant reduction in the phosphorylation of GSK3 protein in P301S;P2X7^{451P}EGFP mice (343 ± 10.4 % lower than in P301S mice, Fig. 5C) and a rise in intracellular phospho-Tau protein levels (37.4 ± 7.0 % higher than P301S mice, Fig. 5D). Noteworthy, P301S;P2X7^{451P}EGFP mice did not show either an increase in positive AT8 neurons nor reduction in the number of hippocampal neurons (Fig. 5E-H). Of note, although P301S;P2X7^{451P}EGFP mice presented significantly lower phosphorylated eTau levels (Fig. 5I), they only showed a tendency, but not a significant increase on TNAP levels (Fig. 5J-K). Unexpectedly, P301S;P2X7^{451P}EGFP mice neither showed an increase in the number of hippocampal microglial and astroglial cells nor a more prominent activation state of microglia, or more IL-1β secretion than P301S mice (Fig. 5J and L and supplementary Fig. 8). These unexpected results may be explained by a basal activation state of the microglial linage in P2X7^{451P}EGFP mice (supplementary Fig. 6), which might affect the grade of Tau-induced microglia activation detected in P301S;P2X7^{451P}EGFP mice.

4. Discussion

In this study, we describe, for the first time, how P2X7 plays a critical role in Tau-induced toxicity by regulating microglia functionality and Tau phosphorylation rate both in the intracellular and extracellular compartments. Supporting this claim, we found that both *in vivo* pharmacological inhibition and genetic knockout of P2X7 revert the microglial activation in P301S mice, leading to a decrease of microglial migratory and secretory capacities, reducing the microglial proliferation and promoting its phagocytic ability. Furthermore, the genetic or pharmacological P2X7 blockade reduced GSK3 enzyme activity, leading to a significant reduction of intraneuronal phosphorylated Tau levels, but also promoted the phosphorylation of eTau by decreasing the TNAP ectoenzyme expression. Accordingly, a reduction of neuronal loss, an improvement in motor and memory capacities, and amelioration in the anxiety profile were observed in P301S mice upon P2X7 blockade. In this line, an additional P2X7 overexpression caused a significant worsening of the Tau induced toxicity in P301S mice aggravating the motor and memory deficits of these mice.

In AD, it is assumed that accumulation of Aβ in senile plaques initiates the inflammatory process (McGeer et al., 2000), by activating surrounding microglial cells (Selkoe, 2002). Therefore, the finding of P2X7 upregulation in microglia cells surrounding the senile plaques in AD patients suggested the involvement of this receptor in microglial activation in an Aβ-dependent way (McLarnon et al., 2006; Parvathenani et al., 2003). However, in the present work besides the P2X7 upregulation in AD patients, as previously reported (McLarnon et al., 2006; Parvathenani et al., 2003; Ryu and McLarnon, 2008), we also found a similar P2X7 upregulation in PiD patients and P301S mice, where a significant Aβ accumulation was not present. In accordance with these results, in a previous work we have reported that LPS-induced neuroinflammation causes a change in P2X7R distribution pattern, increasing its transcription and expression on microglial cells and decreasing it in neurons (Martinez-Frailes et al., 2019). Supporting our findings, different single-nuclei RNA sequencing studies have corroborated that in AD patients microglial cells present elevated *P2RX7* transcript levels while neurons show a clear reduction (Del-Aguila et al., 2019; Grubman et al., 2019). Furthermore, as the pharmacological or genetic blockade of P2X7 in P301S mice re-established the resting state in activated microglia, we postulated that increased P2X7 expression in microglial cells plays a critical role in the activation of this linage in Tauopathies. Supporting this hypothesis, P2X7 overexpressing mice showed microglial cells with a morphology similar to the activated one present in the symptomatic P301S mice. Likewise, previous *in vitro* studies reported that P2X7 overexpression in microglia cells cause both microglial activation and proliferation (Monif et al., 2009). Accordingly, *in vivo* pharmacological or genetic P2X7R blockade reduced microglia activation and proliferation and IL-1β secretion in P301S mice. In this same line Mancuso *et al.* have recently reported that blockage of microglial proliferation led to an attenuation of Tau-induced neurodegeneration resulting in a functional improvement in P301S mice (Mancuso et al., 2019). Besides, we detected lower extracellular ATPase activity and higher Connexin-43 levels in the hippocampus of P301S mice. Both events can promote an increase extracellular ATP levels, and would favor the activated state of the upregulated P2X7s, resulting in chronic microglial activation in P301S mice. In agreement with this hypothesis,

it was reported that the activated microglia, but not microglia in the resting state, overexpresses Connexin-43 (Sanchez et al., 2020). Moreover, an extracellular environment enriched in purines would also favor the activation of other purinergic receptors impacting microglia functionally. For example, adenosine A2A receptor, involved in the retraction of microglial processes occurring during neuroinflammation (Orr et al., 2009). Interestingly, since it was recently reported that P2X7 blockade attenuates the upregulation of A2A receptors in microglial cells (Dias et al., 2021), we cannot discard that some of the beneficial effects induced by P2X7 blockade in P301S mice may be due to their indirect regulation of the A2A receptor. However, additional studies should be done to evaluate this possibility. Altogether our results suggest that P2X7 upregulation in microglial cells is one of the molecular mechanisms causing their chronic activation and proliferation contributing to the neuroinflammation state associated with Tauopathies. Supporting this hypothesis, pharmacological or genetic blockade of P2X7 reduced the anxiety-related behavior of P301S mice. However, since neuroinflammation may also contribute to the depressive-like behavior associated with dementia patients (Korczyn and Halperin, 2009; Zheng et al., 2021), additional studies should be done to evaluate the potential beneficial effect of P2X7 blockage on these behavioral alterations.

In addition to microglia cells, P2X7 was also found in neurons (Miras-Portugal et al., 2017), where it regulates critical functions, such as axonal elongation and branching or APP processing *via* GSK3-β signaling (Diaz-Hernandez et al., 2012, 2008). In accordance with previous *in vitro* studies carried out in cultured hippocampal neurons, we noted that pharmacological or genetic P2X7 blockade reduced the intraneuronal Tau phosphorylation rate by inhibiting GSK3-β in P301S mice (Diaz-Hernandez et al., 2012, 2008). Therefore, involvement of neuronal P2X7 in the beneficial effects described above, can be assumed. Nevertheless, a contribution of microglia to the reduced phosphorylation rate of intraneuronal Tau cannot be ruled out. It has recently been reported that NLRP3 activation induces Tau hyperphosphorylation and aggregation, at least partially through Tau kinases in an IL-1β-dependent manner (Ising et al., 2019). In accordance, another study also reported that IL-1β overexpression promotes Tau phosphorylation in a GSK3-β dependent way (Ghosh et al., 2013). Considering these studies, it is reasonable to think that the decrease in the intraneuronal Tau phosphorylation rate induced by the genetic or pharmacological P2X7 blockade might be caused by the reduction in IL-1β secretion from microglia. In line with these results, we found that P2X7 overexpression is sufficient to increase the intraneuronal phosphorylated Tau levels even in the absence of Tau-induced toxicity. Along these same lines, we found that an P2X7 overexpression aggravated the associated behavioral defects in P301S mice. Nevertheless, P2X7 overexpression neither exacerbated morphological-changes associated with microglial activation nor their proliferation and also did not enhance the IL-1β secretion. Although the basal microglia activation found in P2X7 overexpressing mice might explain the absence of a stronger microglial activation and a more robust IL-1β release in P301S;P2X7^{451P}EGFP mice, additional studies are necessary to clarify this point. Since the observed effects could not be explained considering only the contribution of microglia P2X7, we propose that P2X7 blockade in other cellular linages like neurons could contribute to reducing the intracellular phosphorylated Tau levels.

Several studies have reported that *in vivo* pharmacological blockade or genetic depletion of P2X7 leads to a significant improvement of both symptomatology, and neuropathology in different AD animal models by reducing the APP-induced toxicity (Chen et al., 2014; Diaz-Hernandez et al., 2012; Martin et al., 2019; Ryu and McLarnon, 2008). However, the efficiency of this therapeutic approach to treat Tauopathies has not been evaluated yet. Here, we reported for the first time, that the blockade of P2X7 is a potential therapeutic strategy to treat Tauopathies. Notably, the neuroprotective effect induced by P2X7 blockade was linked to an increase in phosphorylated eTau. Interestingly, a recent work reported that eTau hyperphosphorylation occurs very early in Tauopathies, when cellular loss is not yet detected but decreases significantly near the onset of cognitive decline (Barthelemy et al., 2020). In agreement, previous studies reported that dephosphorylated eTau but not the hyperphosphorylated eTau causes neuronal toxicity (Diaz-Hernandez et al., 2010), and triggers the pro-inflammatory profile in microglia (Perea et al., 2018). Considering these contributions, we can speculate that one of the molecular mechanisms by which P2X7 blockade causes beneficial effects might be by maintaining high levels of the phosphorylated eTau. Supporting this hypothesis, previous studies reported that P2X7 inhibition reduces the TNAP transcription, an ectoenzyme that dephosphorylates the eTau (Diaz-Hernandez et al., 2010; Diez-Zaera et al., 2011). In agreement, we found that the cellular survival induced by genetic deletion or pharmacological blockade of P2X7 was linked with a reduction in TNAP expression and an increase in phosphorylated eTau levels. Furthermore, we found that P2X7 blockade raises the microglial phagocytic capacity, as previously reported (Martinez-Frailes et al., 2019). Since eTau can be taken up by microglia cells (Luo et al., 2015), it is reasonable to think that Tau-induced P2X7 upregulation in microglia cells might contribute to Tauopathy progression by reducing the phagocytosis of eTau. However, additional experiments should be performed to confirm this hypothesis. Conversely, P301S;P2X7^{451P}EGFP mice showed lower phosphorylated eTau levels than P301S mice, but this reduction was not coupled with a significant increase in hippocampal TNAP levels. Since neuroinflammation seems to be a causing factor for the increased TNAP expression, the lack of a more pronounced neuroinflammation in P301S;P2X 7^{451P}EGFP mice suggests that other P2X7-dependent mechanisms might be contributing to the regulation of the phosphorylated eTau levels.

In recent years, different therapeutic strategies, based on targeting directly eTau protein, revealed unexpected results. These clinical trials were focused on reducing the intracellular phosphorylated Tau rate (Dominguez et al., 2012), avoiding Tau aggregation (Wisniewski and Goni, 2015), or promoting Tau removal through active and passive immunotherapy approaches. Nevertheless, active immunotherapy may have harmful effects (Rozenstein-Tsalkovich et al., 2013), and passive immunotherapy, although reducing Tau-induced pathology, failed to increase the life expectancy in Tauopathy mouse models (d'Abramo et al., 2013; Wisniewski and Goni, 2015). Our results show that P2X7 blockage reverted microglial activation, intracellular Tau hyperphosphorylation, improved neuronal survival, and associated-behavioural deficits. Besides, as we used symptomatic mice, our results indicate that this strategy could be effective in order to revert the pathophysiological hallmarks and behavioural alterations associated with Tauopathies, even in symptomatic patients in the advanced stages of the disease. However, we demonstrate the improvement in some aspects of the pathology induced by a three-week treatment with P2X7 antagonist, but additional studies could be done to evaluate if longer treatments maintain or improve even more the pathology.

5. Conclusions

Here, we provide evidence that P2X7 is involved in Tau-dependent pathological processes. Therefore, the behavioural alterations associated with Tauopathies improve or worsen by depleting or augmenting the genetic load of P2X7 in P301S mice respectively. Moreover, using this experimental strategy, we demonstrate for first time that microglial P2X7 plays a critical role in Tau-induced toxicity by regulating microglial cells' functionality. In addition, we found that P2X7 regulates Tau phosphorylation rate in intracellular and extracellular compartments by modulating the GSK3 signalling pathway and TNAP expression, respectively. Furthermore, our studies indicate that the pharmacological P2X7 blockade might be considered a promising treatment for Tauopathies since it reduces neuroinflammation, improves neuronal survival, and ameliorates behavioural deficits associated with these diseases.

Author's contribution

C.dL bred and processed the transgenic mice, generated and analyzed the samples, participated in experimental design, contributed to the interpretation of the data; C.B., B.A-C., and L.S-T. contributed to sample processing; A. S-S and A. N. revised the manuscript and provided essential material; M.D-H. participated in mouse breeding and processing, generated and analyzed the samples, participated in the experimental design, contributed to the interpretation of the results, wrote the manuscript and provided financial support for the work. All authors read and approved the final manuscript.

Funding

This work was supported by funding from the following: Spanish Ministry of Economy and CompetitivenessRTI2018-095753-B-I00 (to M. D.-H.); European Union project H2020-MSCA-ITN-2017 number 766 124 (to M.D-H and A.N); the DFG, Project-ID: 335447717 - SFB 1328 (to A.N.); UCM-Santander Central Hispano BankPR41/17-21014 (to M.D-H). A.S-S was hired by RTI2018-095753-B-I00 grant and currently hired by UCM as postdoctoral researcher (CT48/19), C.dL. and C.B. were hired by H2020-MSCA-ITN-2017 (grant number 766124). B.A-C is funded by the Spanish Ministry of Science and innovation (Ramón y Cajal- RYC2018-024435-I) and by the Autonomous Community of Madrid (Atracción de Talento-2019T1/BMD-14057) grants.

Declaration of Competing Interest

The authors declare no conflict of interest, financial or otherwise.

Appendix A. The Peer Review Overview and Supplementary data

The Peer Review Overview and Supplementary data associated with this article can be found in the online version, at doi: https://doi.org/10.1016/j.pneurobio.2021.102173.

References

Asai, H., Ikezu, S., Tsunoda, S., Medalla, M., Luebke, J., Haydar, T., Wolozin, B., Butovsky, O., Kugler, S., Ikezu, T., 2015. Depletion of microglia and inhibition of exosome synthesis halt tau propagation. Nat. Neurosci. 18, 1584–1593.

Barthelemy, N.R., Li, Y., Joseph-Mathurin, N., Gordon, B.A., Hassenstab, J., Benzinger, T. L.S., Buckles, V., Fagan, A.M., Perrin, R.J., Goate, A.M., Morris, J.C., Karch, C.M., Xiong, C., Allegri, R., Mendez, P.C., Berman, S.B., Ikeuchi, T., Mori, H., Shimada, H., Shoji, M., Suzuki, K., Noble, J., Farlow, M., Chhatwal, J., Graff-Radford, N.R., Salloway, S., Schofield, P.R., Masters, C.L., Martins, R.N., O'Connor, A., Fox, N.C., Levin, J., Jucker, M., Gabelle, A., Lehmann, S., Sato, C., Bateman, R.J., McDade, E., Dominantly Inherited Alzheimer, N, 2020. A soluble phosphorylated tau signature links tau, amyloid and the evolution of stages of dominantly inherited Alzheimer's disease. Nat. Med. 26, 398–407.

Bondareff, W., Mountjoy, C.Q., Roth, M., Hauser, D.L., 1989. Neurofibrillary degeneration and neuronal loss in Alzheimer's disease. Neurobiol. Aging 10, 709–715.

Burnstock, G., 2007. Physiology and pathophysiology of purinergic neurotransmission. Physiol. Rev. 87, 659–797.

Chen, X., Hu, J., Jiang, L., Xu, S., Zheng, B., Wang, C., Zhang, J., Wei, X., Chang, L., Wang, Q., 2014. Brilliant Blue G improves cognition in an animal model of Alzheimer's disease and inhibits amyloid-beta-induced loss of filopodia and dendrite spines in hippocampal neurons. Neuroscience 279, 94–101.

Collins, M.A., An, J., Peller, D., Bowser, R., 2015. Total protein is an effective loading control for cerebrospinal fluid western blots. J. Neurosci. Methods 251, 72–82.

Colonna, M., Butovsky, O., 2017. Microglia function in the central nervous system during health and neurodegeneration. Annu. Rev. Immunol. 35, 441–468.

d'Abramo, C., Acker, C.M., Jimenez, H.T., Davies, P., 2013. Tau passive immunotherapy in mutant P301L mice: antibody affinity versus specificity. PLoS One 8, e62402.

Del-Aguila, J.L., Li, Z., Dube, U., Mihindukulasuriya, K.A., Budde, J.P., Fernandez, M.V., Ibanez, L., Bradley, J., Wang, F., Bergmann, K., Davenport, R., Morris, J.C., Holtzman, D.M., Perrin, R.J., Benitez, B.A., Dougherty, J., Cruchaga, C., Harari, O., 2019. A single-nuclei RNA sequencing study of Mendelian and sporadic AD in the human brain. Alzheimers Res. Ther. 11, 71.

Dias, L., Lopes, C.R., Goncalves, F.Q., Nunes, A., Pochmann, D., Machado, N.J., Tome, A. R., Agostinho, P., Cunha, R.A., 2021. Crosstalk between ATP-P2X7 and Adenosine A2A receptors controlling neuroinflammation in rats subject to repeated restraint stress. Front. Cell. Neurosci. 15, 639322.

Diaz-Hernandez, M., del Puerto, A., Diaz-Hernandez, J.I., Diez-Zaera, M., Lucas, J.J., Garrido, J.J., Miras-Portugal, M.T., 2008. Inhibition of the ATP-gated P2X7 receptor promotes axonal growth and branching in cultured hippocampal neurons. J. Cell. Sci. 121, 3717–3728.

Diaz-Hernandez, M., Diez-Zaera, M., Sanchez-Nogueiro, J., Gomez-Villafuertes, R., Canals, J.M., Alberch, J., Miras-Portugal, M.T., Lucas, J.J., 2009. Altered P2X7-receptor level and function in mouse models of Huntington's disease and therapeutic efficacy of antagonist administration. FASEB J. 23, 1893–1906.

Diaz-Hernandez, M., Gomez-Ramos, A., Rubio, A., Gomez-Villafuertes, R., Naranjo, J.R., Miras-Portugal, M.T., Avila, J., 2010. Tissue-nonspecific alkaline phosphatase promotes the neurotoxicity effect of extracellular tau. J. Biol. Chem. 285, 32539–32548.

Diaz-Hernandez, J.I., Gomez-Villafuertes, R., Leon-Otegui, M., Hontecillas-Prieto, L., Del Puerto, A., Trejo, J.L., Lucas, J.J., Garrido, J.J., Gualix, J., Miras-Portugal, M.T., Diaz-Hernandez, M., 2012. In vivo P2X7 inhibition reduces amyloid plaques in Alzheimer's disease through GSK3beta and secretases. Neurobiol. Aging 33, 1816–1828.

Diez-Zaera, M., Diaz-Hernandez, J.I., Hernandez-Alvarez, E., Zimmermann, H., Diaz-Hernandez, M., Miras-Portugal, M.T., 2011. Tissue-nonspecific alkaline phosphatase promotes axonal growth of hippocampal neurons. Mol. Biol. Cell 22, 1014–1024.

Dominguez, J.M., Fuertes, A., Orozco, L., del Monte-Millan, M., Delgado, E., Medina, M., 2012. Evidence for irreversible inhibition of glycogen synthase kinase-3beta by tideglusib. J. Biol. Chem. 287, 893–904.

Facci, L., Barbierato, M., Zusso, M., Skaper, S.D., Giusti, P., 2018. Serum amyloid A primes microglia for ATP-dependent interleukin-1beta release. J. Neuroinflammation 15, 164.

Ghosh, S., Wu, M.D., Shaftel, S.S., Kyrkanides, S., LaFerla, F.M., Olschowka, J.A., O'Banion, M.K., 2013. Sustained interleukin-1beta overexpression exacerbates tau pathology despite reduced amyloid burden in an Alzheimer's mouse model. J. Neurosci. 33, 5053–5064.

Gomez-Ramos, A., Diaz-Hernandez, M., Cuadros, R., Hernandez, F., Avila, J., 2006. Extracellular tau is toxic to neuronal cells. FEBS Lett. 580, 4842–4850.

Grubman, A., Chew, G., Ouyang, J.F., Sun, G., Choo, X.Y., McLean, C., Simmons, R.K., Buckberry, S., Vargas-Landin, D.B., Poppe, D., Pflueger, J., Lister, R., Rackham, O.J. L., Petretto, E., Polo, J.M., 2019. A single-cell atlas of entorhinal cortex from individuals with Alzheimer's disease reveals cell-type-specific gene expression regulation. Nat. Neurosci. 22, 2087–2097.

Gu, B.J., Wiley, J.S., 2018. P2X7 as a scavenger receptor for innate phagocytosis in the brain. Br. J. Pharmacol. 175, 4195–4208.

Heneka, M.T., McManus, R.M., Latz, E., 2018. Inflammasome signalling in brain function and neurodegenerative disease. Nat. Rev. Neurosci. 19, 610–621.

Ising, C., Venegas, C., Zhang, S., Scheiblich, H., Schmidt, S.V., Vieira-Saecker, A., Schwartz, S., Albasset, S., McManus, R.M., Tejera, D., Griep, A., Santarelli, F., Brosseron, F., Opitz, S., Stunden, J., Merten, M., Kayed, R., Golenbock, D.T., Blum, D., Latz, E., Buee, L., Heneka, M.T., 2019. NLRP3 inflammasome activation drives tau pathology. Nature 575, 669–673.

Jin, H., Han, J., Resing, D., Liu, H., Yue, X., Miller, R.L., Schoch, K.M., Miller, T.M., Perlmutter, J.S., Egan, T.M., Tu, Z., 2018. Synthesis and in vitro characterization of a P2X7 radioligand [(123)I]TZ6019 and its response to neuroinflammation in a mouse model of Alzheimer disease. Eur. J. Pharmacol. 820, 8–17.

Kaczmarek-Hajek, K., Zhang, J., Kopp, R., Grosche, A., Rissiek, B., Saul, A., Bruzzone, S., Engel, T., Jooss, T., Krautloher, A., Schuster, S., Magnus, T., Stadelmann, C., Sirko, S., Koch-Nolte, F., Eulenburg, V., Nicke, A., 2018. Re-evaluation of neuronal P2X7 expression using novel mouse models and a P2X7-specific nanobody. Elife 7.

Korczyn, A.D., Halperin, I., 2009. Depression and dementia. J. Neurol. Sci. 283, 139–142.

Lee, V.M., Goedert, M., Trojanowski, J.Q., 2001. Neurodegenerative tauopathies. Annu. Rev. Neurosci. 24, 1121–1159.

Luo, W., Liu, W., Hu, X., Hanna, M., Caravaca, A., Paul, S.M., 2015. Microglial internalization and degradation of pathological tau is enhanced by an anti-tau monoclonal antibody. Sci. Rep. 5, 11161.

Mancuso, R., Fryatt, G., Cleal, M., Obst, J., Pipi, E., Monzon-Sandoval, J., Ribe, E., Winchester, L., Webber, C., Nevado, A., Jacobs, T., Austin, N., Theunis, C., Grauwen, K., Daniela Ruiz, E., Mudher, A., Vicente-Rodriguez, M., Parker, C.A., Simmons, C., Cash, D., Richardson, J., Consortium, N., Jones, D.N.C., Lovestone, S., Gomez-Nicola, D., Perry, V.H., 2019. CSF1R inhibitor JNJ-40346527 attenuates microglial proliferation and neurodegeneration in P301S mice. Brain 142, 3243–3264.

Maphis, N., Xu, G., Kokiko-Cochran, O.N., Jiang, S., Cardona, A., Ransohoff, R.M., Lamb, B.T., Bhaskar, K., 2015. Reactive microglia drive tau pathology and contribute to the spreading of pathological tau in the brain. Brain 138, 1738–1755.

Martin, E., Amar, M., Dalle, C., Youssef, I., Boucher, C., Le Duigou, C., Bruckner, M., Prigent, A., Sazdovitch, V., Halle, A., Kanellopoulos, J.M., Fontaine, B., Delatour, B., Delarasse, C., 2019. New role of P2X7 receptor in an Alzheimer's disease mouse model. Mol. Psychiatry 24, 108–125.

Martinez-Frailes, C., Di Lauro, C., Bianchi, C., de Diego-Garcia, L., Sebastian-Serrano, A., Bosca, L., Diaz-Hernandez, M., 2019. Amyloid peptide induced neuroinflammation increases the P2X7 receptor expression in Microglial Cells, impacting on its functionality. Front. Cell. Neurosci. 13, 143.

McGeer, P.L., McGeer, E.G., Yasojima, K., 2000. Alzheimer disease and neuroinflammation. J. Neural Transm. Suppl. 59, 53–57.
McLarnon, J.G., Ryu, J.K., Walker, D.G., Choi, H.B., 2006. Upregulated expression of purinergic P2X(7) receptor in Alzheimer disease and amyloid-beta peptide-treated microglia and in peptide-injected rat hippocampus. J. Neuropathol. Exp. Neurol. 65, 1090–1097.
Miras-Portugal, M.T., Sebastian-Serrano, A., de Diego Garcia, L., Diaz-Hernandez, M., 2017. Neuronal P2X7 receptor: involvement in neuronal physiology and pathology. J. Neurosci. 37, 7063–7072.
Monif, M., Reid, C.A., Powell, K.L., Smart, M.L., Williams, D.A., 2009. The P2X7 receptor drives microglial activation and proliferation: a trophic role for P2X7R pore. J. Neurosci. 29, 3781–3791.
Monif, M., Burnstock, G., Williams, D.A., 2010. Microglia: proliferation and activation driven by the P2X7 receptor. Int. J. Biochem. Cell Biol. 42, 1753–1756.
Ni, J., Wang, P., Zhang, J., Chen, W., Gu, L., 2013. Silencing of the P2X(7) receptor enhances amyloid-beta phagocytosis by microglia. Biochem. Biophys. Res. Commun. 434, 363–369.
Orr, A.G., Orr, A.L., Li, X.J., Gross, R.E., Traynelis, S.F., 2009. Adenosine A(2A) receptor mediates microglial process retraction. Nat. Neurosci. 12, 872–878.
Parvathenani, L.K., Tertyshnikova, S., Greco, C.R., Roberts, S.B., Robertson, B., Posmantur, R., 2003. P2X7 mediates superoxide production in primary microglia and is up-regulated in a transgenic mouse model of Alzheimer's disease. J. Biol. Chem. 278, 13309–13317.
Perea, J.R., Avila, J., Bolos, M., 2018. Dephosphorylated rather than hyperphosphorylated Tau triggers a pro-inflammatory profile in microglia through the p38 MAPK pathway. Exp. Neurol. 310, 14–21.
Rigato, C., Swinnen, N., Buckinx, R., Couillin, I., Mangin, J.M., Rigo, J.M., Legendre, P., Le Corronc, H., 2012. Microglia proliferation is controlled by P2X7 receptors in a Pannexin-1-independent manner during early embryonic spinal cord invasion. J. Neurosci. 32, 11559–11573.
Roh, J.S., Sohn, D.H., 2018. Damage-associated molecular patterns in inflammatory diseases. Immune Netw. 18, e27.
Rozenstein-Tsalkovich, L., Grigoriadis, N., Lourbopoulos, A., Nousiopoulou, E., Kassis, I., Abramsky, O., Karussis, D., Rosenmann, H., 2013. Repeated immunization of mice with phosphorylated-tau peptides causes neuroinflammation. Exp. Neurol. 248, 451–456.
Ryu, J.K., McLarnon, J.G., 2008. Block of purinergic P2X(7) receptor is neuroprotective in an animal model of Alzheimer's disease. Neuroreport 19, 1715–1719.
Sanchez, O.F., Rodriguez, A.V., Velasco-Espana, J.M., Murillo, L.C., Sutachan, J.J., Albarracin, S.L., 2020. Role of connexins 30, 36, and 43 in brain tumors, neurodegenerative diseases, and neuroprotection. Cells 9.
Sanz, J.M., Chiozzi, P., Ferrari, D., Colaianna, M., Idzko, M., Falzoni, S., Fellin, R., Trabace, L., Di Virgilio, F., 2009. Activation of microglia by amyloid {beta} requires P2X7 receptor expression. J. Immunol. 182, 4378–4385.
Sebastian-Serrano, A., Engel, T., de Diego-Garcia, L., Olivos-Ore, L.A., Arribas-Blazquez, M., Martinez-Frailes, C., Perez-Diaz, C., Millan, J.L., Artalejo, A.R., Miras-Portugal, M.T., Henshall, D.C., Diaz-Hernandez, M., 2016. Neurodevelopmental alterations and seizures developed by mouse model of infantile hypophosphatasia are associated with purinergic signalling deregulation. Hum. Mol. Genet. 25, 4143–4156.
Sebastian-Serrano, A., de Diego-Garcia, L., Diaz-Hernandez, M., 2018a. The neurotoxic role of extracellular tau protein. Int. J. Mol. Sci. 19.
Sebastian-Serrano, A., de Diego-Garcia, L., Henshall, D.C., Engel, T., Diaz-Hernandez, M., 2018b. Haploinsufficient TNAP mice display decreased extracellular ATP levels and expression of Pannexin-1 channels. Front. Pharmacol. 9, 170.
Selkoe, D.J., 2002. Alzheimer's disease is a synaptic failure. Science 298, 789–791.
Skaper, S.D., Facci, L., Zusso, M., Giusti, P., 2018. An inflammation-centric view of neurological disease: beyond the neuron. Front. Cell. Neurosci. 12, 72.
Territo, P.R., Meyer, J.A., Peters, J.S., Riley, A.A., McCarthy, B.P., Gao, M., Wang, M., Green, M.A., Zheng, Q.H., Hutchins, G.D., 2017. Characterization of (11)C-GSK1482160 for targeting the P2X7 receptor as a biomarker for neuroinflammation. J. Nucl. Med. 58, 458–465.
Wisniewski, T., Goni, F., 2015. Immunotherapeutic approaches for Alzheimer's disease. Neuron 85, 1162–1176.
Yoshiyama, Y., Higuchi, M., Zhang, B., Huang, S.M., Iwata, N., Saido, T.C., Maeda, J., Suhara, T., Trojanowski, J.Q., Lee, V.M., 2007. Synapse loss and microglial activation precede tangles in a P301S tauopathy mouse model. Neuron 53, 337–351.
Young, K., Morrison, H., 2018. Quantifying microglia morphology from photomicrographs of immunohistochemistry prepared tissue using ImageJ. J. Vis. Exp.
Zheng, Z.H., Tu, J.L., Li, X.H., Hua, Q., Liu, W.Z., Liu, Y., Pan, B.X., Hu, P., Zhang, W.H., 2021. Neuroinflammation induces anxiety- and depressive-like behavior by modulating neuronal plasticity in the basolateral amygdala. Brain Behav. Immun. 91, 505–518.